

Scale test facility for measuring vortex induced vibrations

Jiayao Sun

Technische Universiteit Delft



Scale test facility for measuring vortex induced vibrations

BY

Jiayao Sun

A thesis submitted in partial fulfilment of the requirement for the
degree of

MASTER OF SCIENCE

IN

OFFSHORE AND DREDGING ENGINEERING

at the

Delft University of Technology

2017-06-19

Abstract

The main objective of this dissertation is to compare the small-scaled model test by the flume with the full-scaled model test carried out by the towing tank and to find out the differences between the test results and the test facilities to give proper suggestions for the design and operation on small-scaled testing facilities.

The methodology used in this dissertation is carried out on the small-scaled model test in the flume. Three main steps are carried out, the first is comparing the test results of the flume and the towing tank for both the stationary test and the free vibration test, the second is looking for the theoretical explanations of the differences between the test results, the third is finding out the advantages and disadvantages of the small-scaled model testing facility compared with the full-scaled model test results which have been carried out by the towing tank in the previous research. After the model test, the wake oscillator model is also used simulate the real model test and find out the influence of different parameters on the test results.

The main conclusions of this dissertation is that for small-scaled model test carried out in the flume, the free vibration tests match the full-scaled model well, which can be used to evaluate the vibration suppression efficiency of the strake model. In the stationary test, the small-scaled model provides higher drag coefficient due to the difference of Reynolds number. In the numerical model, the parameters which may influence the oscillating amplitudes are the tuning parameters. And the different series of tuning parameters are given according to the spring stiffness.

Acknowledgement

My deepest gratitude goes first and foremost to Professor A.V. Metrikine, my committee chairman, for his constant encouragement and guidance. He has walked me through all the stages of the writing of this thesis. Without his consistent and illuminating instruction, this thesis could not have reached its present form.

Second, I would like to express my heartfelt gratitude to Mr. Yang Qu, who led me into the wake oscillator theory and guide me on the thesis writing. I am also greatly indebted to my company supervisor Mr. Karst Meijer and Mr. A. van Belkom from Lankhorst, for offering valuable advice and guidance in my writing, and whose intellectual insights have contributed greatly to the completion of this thesis.

Last my thanks would go to my beloved family for their loving considerations and great confidence in me all through these years. I also owe my sincere gratitude to my friends and my fellow classmates who gave me their help and time in listening to me and helping me work out my problems during the difficult course of the thesis.

My special thanks also go to all my teachers whose inspiring lectures have had an undoubted influence on much of the content of my thesis. I would like to extend my heartfelt gratitude to the authors whose words I have cited or quoted, and to the scholars upon whose ideas I have freely drawn.

Content

Abstract.....	III
Acknowledgement	V
Content	VII
List of Figures	IX
List of Tables.....	XI
Nomenclature	XIII
1. Introduction	1
1.1. An Overview of the Topic	1
1.2. Target and Objectives.....	1
1.3. Guide to the Contents.....	2
2. Literature Review.....	4
2.1. Mass Ratio.....	4
2.2. Damping	7
2.3. Reynolds Number	9
2.4. Long Flexible Cylinder	11
2.5. Surface Roughness	13
2.6. Summary of Literature Review	15
3. Set Up of Experiment.....	17
3.1. Experiment Facilities and Set Up	17
3.2. Data Analysis	23
3.3. Stationary Test Results	30
3.4. Free Vibration Test Results	32
4. Comparison and analysis	36
4.1. MARIN	36
4.2. OCEANIC	43
4.3. Summery	47
5. Wake Oscillator Model.....	49
5.1. Introduction	49
5.2. Wake Oscillator Model.....	49
5.3. Free Vibration Simulation	51
5.4. Range of Application.....	52
5.5. Tuning Parameter in Different Experiments	55

5.6.	Summary	61
6.	Testing Facilities Design	62
6.1.	Comparison of the Flume and Towing Tank	62
6.2.	Flow Rate.....	66
6.3.	Flume Size	68
6.4.	Suggestions	69
7.	Conclusion and Recommendation.....	72
7.1.	Conclusion	72
7.2.	Recommendation.....	72
	Reference	73
	Appendix A.....	75
	Appendix B	79

List of Figures

Figure 1 Critical Mass Ratio[1]	5
Figure 2 Effect of Mass Ratio[2]	6
Figure 3 Modes of Response [3]	7
Figure 4 Effect of Damping[5].....	8
Figure 5 Design Curves of Griffin Plot[8].....	10
Figure 6 Drag Coefficient for Single Cylinder in Cross Flow at Carious Surface Roughness Parameters[9].....	11
Figure 7 Set-up of Experiment[10]	12
Figure 8 Trajectories of Different Part[10]	12
Figure 9 Expression of Phase Angle[10]	13
Figure 10 Equal/Different Phase Angles[10]	13
Figure 11 Base Cd vs. Rn for Different Cylinder Models[11]	14
Figure 12 Oscillating Amplitude for Different Surface Roughness[11]	14
Figure 13 Load Cell Combination for Stationary Experiment.....	19
Figure 14 Free Vibration Experiment	20
Figure 15 The models before cutting.....	21
Figure 16 Cutting the Cover	21
Figure 17 Covers with Cylinder	22
Figure 18 Strakes with Cylinder	22
Figure 19 Example of Acquisition and Proccession	23
Figure 20 Amplifier	23
Figure 21 Delta Elektronika, Dual Power Supply E018-0.6D.....	24
Figure 22 A/D Converter Made by Water Lab	25
Figure 23 Data matrix for free vibration test.....	25
Figure 24 Data Matrix for Stationary Test.....	26
Figure 25 FFT results for one test at Q_400_Forces with Frequency Filter 10Hz	28
Figure 26 FFT result for Q_455_Force with Frequency Content at 5Hz.....	29
Figure 27 Main Drag Coefficient for Stationary Test	31
Figure 28 Oscillation Drag Coefficient for Stationary Test.....	31
Figure 29 Oscillation Lift Coefficient for Stationary Test.....	32
Figure 30 Strouhal Number for Stationary Test.....	32
Figure 31 Amplitude of Oscillations for Free Vibration Test	33
Figure 32 Oscillation Amplitude of Small-scaled Strake Model.....	34
Figure 33 Oscillation Frequency for Free Vibration Test	34
Figure 34 Mean Drag for Free Vibration Test.....	35
Figure 35 Oscillation Drag for Free Vibration Test	35
Figure 36 Types of Test	36
Figure 37 Original Results from MARIN.....	37
Figure 38 Selected Results for Bare Pipe and Strakes.....	38
Figure 39 Test Results from Water Lab	39
Figure 40 Merged Test Result	39
Figure 41 Mean Drag Coefficient Uncorrected.....	40

Figure 42 Mean Drag with Uncorrected Small-scaled Results	40
Figure 43 Mean Drag Coefficient with Blockage Correction	41
Figure 44 Drag Coefficient of Single Cylinder at Various Roughness [9].....	41
Figure 45 Effect of Blockage Correction for Large-scaled Model	43
Figure 46 Effect of Blockage Correction for Small-scaled Model.....	43
Figure 47 Mean Drag Coefficient-OCEANIC.....	44
Figure 48 Merged Drag Coefficient without Blockage Correction	45
Figure 49 Amplitude of Oscillation.....	45
Figure 50 Amplitude of Oscillation.....	46
Figure 51 Amplitude of Oscillation (Merged)	46
Figure 52 Oscillation Amplitude of Strake	47
Figure 53 Definition of Angle and Forces[20]	50
Figure 54 Wake Oscillator for 20-seconds' Simulation.....	51
Figure 55 Wake Oscillator Simulation for Bare Pipe Test	52
Figure 56 Wake Oscillator Simulation for Cover	52
Figure 57 Effect of Mass Ratio on Wake Oscillator Model.....	53
Figure 58 Effect of Damping Ration on Wake Oscillator Model	54
Figure 59 Effect of tuning parameter A	55
Figure 60 Effect of Tuning Parameter ε	55
Figure 61 Experiment from Blevins (2009).....	56
Figure 62 Experiment Results from Lee and Bernitsas (2011)[6]	57
Figure 63 Experiment of Lee, Bemitsas(2011), Switch the Reynolds Number Into Reduced Velocity	58
Figure 64 Wake Oscillator Simulation under Reduced Velocity	59
Figure 65 Wake Oscillator Simulation under Constant Tuning Parameters.....	59
Figure 66 Wake Oscillator Simulation for k=1800N/m under Reduced Velocity	60
Figure 67 Synchronisation Regime with Mass Ratio	67
Figure 68 Calculating procedure	67
Figure 69 Air Bearings for Free Vibration Test Facility[21]	69
Figure 70 Two Degrees of Freedom Testing Facility.....	70
Figure 71 Rotation Rig for Fairing Model[23]	71

List of Tables

Table 1 Damping for Run 3.....	8
Table 2 Range of Reynolds Number[7]	9
Table 3 Test List for the Entire Experiment.....	17
Table 4 SCAIME Load Cell Test	18
Table 5 Arrangement for Load Cell in Free Vibration Test.....	18
Table 6 Load Cell Arrangement for Stationary Test.....	19
Table 7 Optic Laser	19
Table 8 Frictionless Table	20
Table 9 Delta Dual Power	24
Table 10 Channels for Free Vibration Test	25
Table 11 Channels for Stationary Test.....	25
Table 12 Natural Frequency of Models in Water	32
Table 13 Total Test Model from MARIN	36
Table 14 Test Results for Bare Pipe and Strakes.....	38
Table 15 Range of Reynolds Number on Each Test	58
Table 16 Combination of Tuning Parameters	60
Table 17 The Comparison of the Large and Small Scaled Model Test	64
Table 18 Large and Small Scaled Fairing Model Test.....	65

Nomenclature

Abbreviations

Abbreviation	Description
ADC	Analogue/Digital converter
VMEC	Variable magnetic eddy-current damping system
DOF	Degree of freedom
FFT	Fast Fourier transform
VIV	Vortex induced vibration
Visc	Viscous flow current

Greek Symbols

Symbol	Description	Unit
α	Mass-damping ratio	[m]
ρ	Fluid density	[kg/m ³]
π	Constant, ratio of a circle's circumference to its diameter	[-]
ζ	Damping ratio	[-]
Δt	Time step	[s]
σ_{Displ}	Standard deviation of the oscillating displacement	[m]
η	Strake efficiency	[-]

Latin Symbols

Symbol	Description	Unit
A	Amplitude of oscillation	[m]
A^*	Reduced amplitude of oscillation	[-]
C_A	Ratio of added mass	[-]
C_d	Drag coefficient	[-]
C'_d	Measured value of drag coefficient	[-]
D	Diameter of the cylinder	[m]
$f_{Nyquist}$	Nyquist frequency	[Hz]
f^*	Reduced oscillating frequency	[-]
K	Spring stiffness	[N/m]
L	Length of the cylinder	[m]
m	Mass of oscillator	[kg]
m^*	Mass ratio	[-]
m^*_{CRIT}	Critical mass ratio	[-]
Re	Reynolds number	[-]
Re_{crit}	Critical Reynolds number	[-]
St	Strouhal number	[-]

T	Measuring time	[s]
U^*	Reduced velocity	[-]
U_{end}^*	Upper boundary of synchronisation regime	[-]
ν	Dynamic viscosity of fluid	[m ² /s]
Vr	Reduced velocity	[-]

1. Introduction

1.1. An Overview of the Topic

In the production of offshore platforms, risers act as transporters which transport the crude oil or the gas from the wells at sea bottom to the production platform or FPSO.

While the riser is placed in the sea, the current will flow around the riser, which causes vortex. The fluid force acting on the riser can be divided into two parts, the lift force which is normal to the flow direction and the drag force which is parallel with the flow. When the flow rate increases to a certain level, the vortex-induced vibration (VIV) happens, which is the main influencing factor on the fatigue life of the riser.

The main VIV suppression methods used in the offshore engineering are the helical strakes and the VIV fairings. However, each of them has its own advantages and disadvantages. For the helical strakes, the suppression is highly effective, but the drag load due to the strakes is also higher than other suppression methods. While for the fairings, the present design may cause even higher vibration amplitudes when the current is at a certain speed. Thus, both models need to be optimised. To evaluate the optimisation, the model testing result is a reliable reference and support for the designer.

There are two types of model testing which are commonly used when evaluating the suppression efficiency. The first one is the large-scaled model test, which tests the real strakes or fairings with the help of the towing tank. The other one is the small-scaled model, which is tested in the flume with the scaled model.

The small scaled model testing facilities have a relative lower cost and higher efficiency when compared with the large scaled model testing facilities. But it is still unknown whether the small scaled model test can give the same results as the large scaled model test, which will be discussed in this dissertation. In this dissertation, we will give suggestions on important parameters that influence the small scaled model testing results, and indicate the proper testing facilities for different type of model.

1.2. Target and Objectives

The aim of this dissertation is to find the advantages and disadvantages of the small-scaled model test by the flume, to make the comparison with the large-scaled model test carried out in the towing tank, and to give suggestions on the design and operation of the flume test.

Two types of test will be done in the flume for the evaluation of the flume, one is the stationary test, and the other is the free vibration test. The test results will be compared with the previous large-scaled model test to find out whether the accuracy on the small-scaled model test will meet the demand.

After the comparison and analysis of the small-scaled model test and the large-scaled model test, suggestions will be given for the future design and operation on the small-scaled model test.

With the comparison between different scale model tests, it is easy to find out whether the small-scaled model testing facility is accurate enough for the estimation or not. However, through the literature study, one may find that there are more mechanisms that can influence the testing results. Besides, it is not convincing enough to conclude that the small and large-scaled model testing has the same or similar accuracy by only one or two experiments.

In this dissertation, through the literature we find the key parameters that influence the model test results, and verify whether the wake oscillator model can simulate the same trend in the real model test, then analyse the advantage and disadvantage of the wake oscillator model. Considering the fact that the wake oscillator model cannot simulation the influence of Reynolds number, we study how the tuning parameters of the wake oscillator model will change according to different Reynolds number.

1.3. Guide to the Contents

The first part of the dissertation is the literature review. In the literature review, one may find the main mechanisms that will influence the vortex induced vibration, such as the mass ratio, damping ratio and Reynolds number, along with the common methods used in the research along with the latest testing equipment.

After the literature review, the next part is the introduction of the small-scaled model testing flume and the testing procedures, coming with the test results. This part is related to the small-scaled model test carried out in the flume from the Water Lab at TU Delft. The small-scaled model is provided by Lankhorst using 3D printing, including the helical strakes model scaled down according to the diameter of the cylinder used in the flume, and the cover is a sleeve without helical strakes. There are two types of testing carried out for this dissertation, one is the stationary test, and the other is free vibration test. In each type of the test, three models are tested, which includes the bare pipe, the cover and the strakes. The bare pipe test is the original cylinder in the flume with a diameter of 40mm, the cover and strakes are scale down to meet the diameter of the cylinder. Each test is repeated three times to increase the reliability on the test results.

In the comparison of the large-scaled model test and the small-scaled model test, the test results such as the drag coefficient and the oscillating amplitude are the main concern in the evaluation of models.

The wake oscillator model is a numerical model which is used to study the free vibration of the oscillator under one degree of freedom. In this dissertation, the relationship between the tuning parameters and the characters such as the mass ratio, damping ratio and Reynolds number will be studied, suggestions on the choosing and the trend are reviewed of the tuning parameters of the wake oscillator model.

With the upon experiment and analysis, the last chapter will give suggestions on the flume design and operation in the future, and with list the advantages and disadvantages of the small-scaled model testing facility to provide the reference for the selection of model testing.

2. Literature Review

Before carrying out the small-scaled model test, it is important to find out how the vortex induced vibration is caused, and which indexes will be used to describe the VIV and how to evaluate its influence on the model. Besides, it is also important to have a good understanding of the current testing methods for both the large-scaled model testing and small-scaled model testing, which includes the advantages and disadvantages of the methodology.

Through the literature review, one can find out the key factors that influence the vortex induced vibration, and the previous studies about the interaction between the characters. For example, in the study of Reynold number, in the common sense the drag force is increased when the flow speed increases. For drag coefficient, one may find that in the research, the drag coefficient for a cylinder experienced two different trends, before the flow speed reaches the critical Reynolds number, the drag coefficient is decreasing. For the super-critical regime of the Reynolds number, the drag coefficient increases with the flow speed.

For the comparison of the two types of experiment, it is important to know which characters will influence the VIV test results most, and which characters can be neglected or play a less important roles. In the literature review, one may find out different testing methods or the testing procedure used for the large-scaled model and the small-scaled model, which lies in the difference between flume test with the towing tank test, respectively.

Except for the different testing procedure for the different scale model, the literature review also indicates some advanced testing methods used in the small-scaled test. For example, the testing facility used in this dissertation has a limited control of the spring stiffness and the damping of the oscillating system. And the friction force or the resistance force in the oscillating system makes the available range of spring stiffness quite limited, it is found during the experiment that when the stiffness is increased, there will be no oscillation at all, even if the flow speed has reached the upper limit of the flume. Due to the limitation of the stiffness range, the small-scaled model is tested under one spring stiffness in the free vibration test. Except for the spring stiffness, the system damping is also unchangeable during the experiment. In the dissertation, to find out how these parameters may influence the VIV test, a numerical model based on the wake oscillator theory is built. It can simulate the oscillation under different spring stiffness and other tuning parameters such as the damping ratio. The results of the simulation will be compared with the relation found in the literature review.

Thus, through the literature review, the main characters that influence the vortex induced vibration and the small-scaled model testing will be determined, which will be used for giving suggestions for the future experiment design.

2.1. Mass Ratio

The Mass ratio is defined as:

$$m^* = \frac{m}{\frac{\pi D^2}{4} \rho L} \quad \text{Equation 1}$$

Where m is the mass of the oscillator, D is the diameter of the cylinder, L is the length of the cylinder and ρ is the density of fluid. For the small-scaled model and the large-scaled model, the mass ratio of each model is different, and in this chapter, we will introduce the effect of mass ratio on the oscillating amplitude and the lock-in range.

2.1.1. Critical Mass Ratio

Govardhan & Williamson (2004)[1] concluded that a critical mass ratio exists as:

$$m_{CRIT}^* = 0.54 \pm 0.02 \quad \text{Equation 2}$$

In the experiment, any mass ratio below this m_{CRIT}^* means that the lower branch of response can never be reached for finite reduced velocities U^* . In other words, the critical mass ratio can be used to define the finite synchronisation regimes of the reduced velocity. These conditions are applicable for finite (U^*/f^*) , so when the mass of the structure falls below the critical value, one predicts that large amplitude vibrations will be experienced under reduced velocity U^* extending to infinity:

$$U_{end\ of\ synchronization}^* = 9.25 \sqrt{\frac{m^* + C_3}{m^* - 0.54}} \quad \text{Equation 3}$$

This expression of the U_{end}^* marks the upper boundary of the shaded synchronisation regime in the following figure. The critical mass ratio $m_{CRIT}^* = 0.54$ as shown in the figure is in the realm of the “relative densities” of full-scale structures in engineering. It means that if the mass ratio of the oscillator is smaller than 0.54, then the synchronisation will not be ended by increasing the reduced velocity.

This critical mass ratio is under the low mass-damping condition, which requires $(m^* + C_A)\zeta < 0.05$. In high mass-damping condition, this critical mass ratio is not applicable.

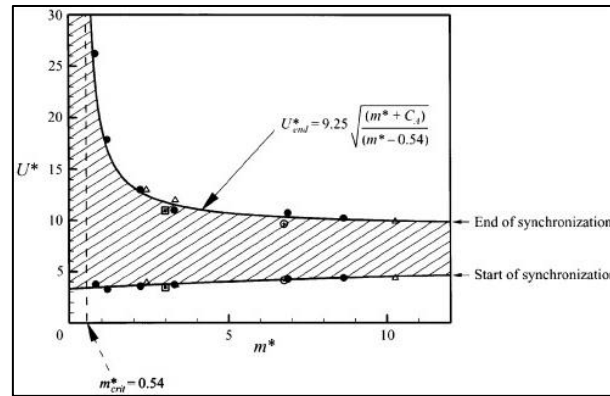


Figure 1 Critical Mass Ratio[1]

By checking the mass ratio of the testing system and comparing it with the synchronisation plot, one can estimate the required reduced velocity for the testing to perform the start and the end of the synchronisation. This will be helpful to define the required flow or tow velocity for the experiment.

2.1.2. Effect of Mass Ratio

In the experiment from Blevins & Coughran (2009)[2], one can find that effect of mass ratio to the synchronisation regime by making higher U^* for lock-in and lower U^* for lock-out. Remains the mass-damping to be constant, when we only increase the mass of the oscillator, the amplitude of oscillation does not change much, while the regime of synchronisation is reduced.

In the figure it is clear to find that while the $m/\rho D^2$ is smaller, the synchronisation regime is wider, with $m/\rho D^2$ continues to increase, the reduced velocity for lock-out will become larger and out of the measured range.

When increases the mass, which means increase the $m/\rho D^2$, the synchronisation regime will become narrow, besides, the beginning of lock-in will be postponed and the lock-out will be earlier. For the small-scaled model test, considering the limited displacement of the cylinder and the total mass of the oscillator, it is hard to achieve the low mass condition for the large-scaled model test.

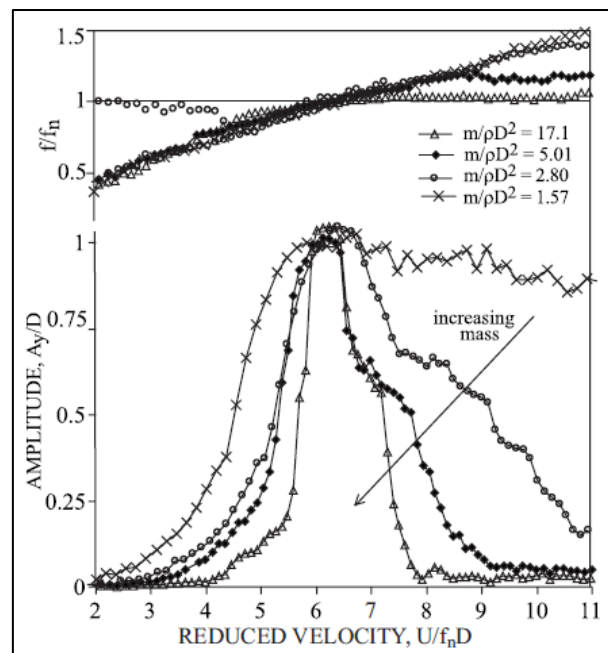


Figure 2 Effect of Mass Ratio[2]

Taking the plot of $m/\rho D^2 = 1.57$ for example, considering the plot of critical mass ratio, when the synchronisation regime for mass ratio m^* is around 1, the upper regime of the synchronisation for U^* is around 20, which is far beyond the maximum reduced velocity achieved in the experiment.

Compared to the mass, the system resistance of the small-scaled model test will also influence the synchronisation regime and the amplitude of the oscillation as the system is sensitive to the change of resistance compared to the towing tank. For free vibration test in small-scaled model, if the mass ratio is too high, there may be no oscillation observed for the whole test. And the resistance of the system will make the vortex harder to “drive” the cylinder—postpone the “lock-in”.

2.2. Damping

2.2.1. Damping with Mass

The mass-damping ($m^*\zeta$) is defined by the mass ratio (m^*) and the damping (ζ), and is divided into two distinct types of response such as the high mass-damping and the low mass-damping proposed by Khalak & Williamson (1999)[3]. This high and low of the mass-damping can be shown through the response mode, which can be found in the following figure.

As it can be seen, for the high mass-damping condition, there are only two modes of response (initial excitation branch, lower branch), while for the low mass-damping condition, there are three modes of response (initial excitation branch, upper branch, lower branch).

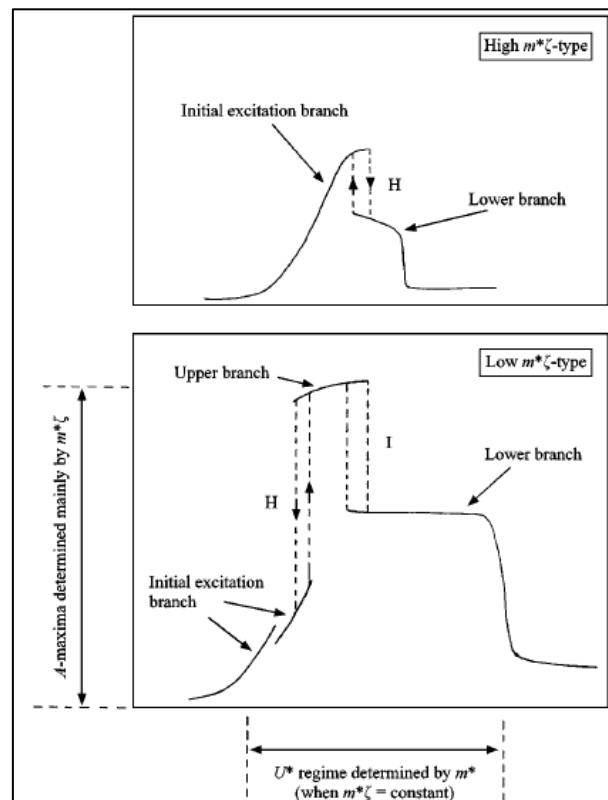


Figure 3 Modes of Response [3]

The amplitude of the oscillation changes with the mass-damping ($m^*\zeta$), and the length of the lock-in regime is determined by the mass ratio (m^*) when the mass-damping ($m^*\zeta$) is constant. Besides, the maximum amplitude of the oscillation is also determined mainly by the mass-

damping ($m^*\zeta$).

The damping of the towing test facility and the flume tests are hard to estimate, in OCEANIC's large-scaled model test, there is only statements that several damping elements were found, but cannot be estimated by percentage. For the Water Lab test of small-scaled model test, we estimate the damping as 2% ($\zeta = 0.02$).

2.2.2. Effect of Damping

To figure out how the damping influences the type of oscillation from three-branch response to the two-branch response, Klamo (2006)[5] used a variable magnetic eddy-current (VMEC) damping system.

With the controlled damper, the following figure shows different oscillation types by changing the damper from low damping as Run 3(a), to high damping as Run 3(j) in the following figure. It shows that by increasing the damping, except for the changing on oscillation shape, the amplitude of oscillation is decreased as well as the synchronisation regime.

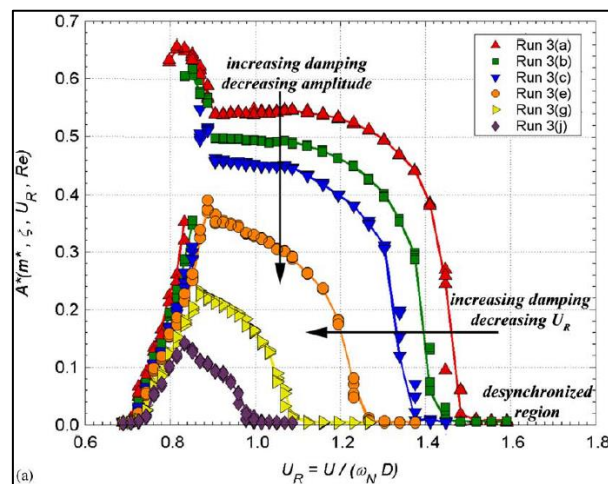


Figure 4 Effect of Damping[5]

The details of the damping coefficients in each run is shown in the following table:

Table 1 Damping for Run 3	
Run	Damping Ratio ζ
3(a)	0.0006
3(b)	0.0015
3(c)	0.0026
3(e)	0.0051
3(g)	0.0085
3(j)	0.0122

2.3. Reynolds Number

2.3.1. Range of Reynolds Number

To divide the Reynolds number more specific and easy to be understood, Pastò (2008)[7] gave a brief introduction to the range of Reynolds number and the condition of the water flow. The following chart shows 4 regimes of Re and 8 different descriptions of flow conditions.

Table 2 Range of Reynolds Number[7]

Re	Regime	Description of Water Flow
$Re = 5$	\	Flow does not detach from the surface of the cylinder; the fluid follows the cylinder contours
$5 \leq Re \leq 45$	\	Flow separates from the back of the cylinder and the near wake is characterized by a symmetric pair of vortices
$45 < Re < 150$	\	Wake becomes unstable and the vortices shed alternately from the cylinder sides. Vortex street, laminar.
$150 \leq Re \leq 300$	\	Wake becomes turbulent, boundary layer on the cylinder remains laminar.
$300 < Re \leq 1.5 \times 10^5$	Subcritical range	Vortex shedding is strong and periodic
$1.5 \times 10^5 < Re \leq 3.5 \times 10^6$	Transitional regime	Cylinder boundary layer becomes turbulent, average drag coefficient decreases
$3 \times 10^5 < Re \leq 3.5 \times 10^6$	Critical subrange	Vortex shedding disappears completely
$Re > 3.5 \times 10^6$	Supercritical regime	Coherent vortex is established again, boundary layer of the cylinder surface is turbulent, the turbulent flow separation points moves forward→drag coefficient increases

For most of the small-scaled model tests, as we can find from the chart, are carried out in the subcritical regime of Re ($300 < Re \leq 1.5 \times 10^5$). For example, in our test with the cylinder diameter of 40mm, the Reynolds number is $5 \times 10^3 < Re < 2 \times 10^4$, which is within the subcritical range. While for the full-scaled model test with cylinder diameter of 324mm, the Reynolds number is $1 \times 10^4 < Re < 8 \times 10^4$.

2.3.2. Effect of Reynolds Number

1) Amplitude of Oscillation

As shown in many experiments, the effect of Reynolds number on the amplitude of oscillation is to increase the highest amplitude of oscillation during the test when other parameters are kept unchanged.

For example, Govardhan and Williamson (2006)[8] defined a “modified Griffin plot”[8] for a steady Reynolds at $1500 < Re < 3.3 \times 10^4$ and a mass-damping < 1.2 , which expressed the relation between the amplitude of oscillation ($A^* = A/D$) and the mass-damping ($\alpha = m^* \times \zeta$) in

different Reynolds number.

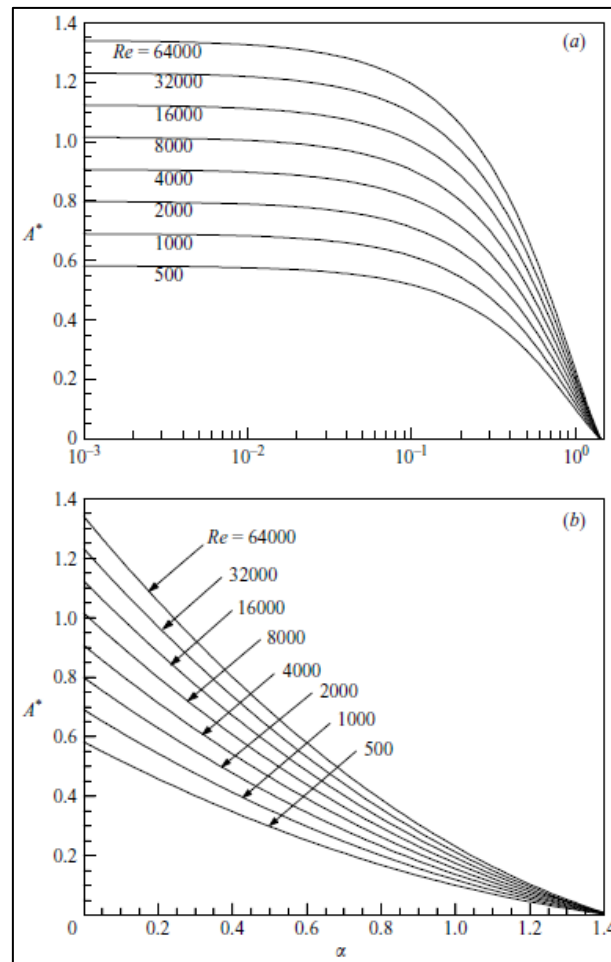


Figure 5 Design Curves of Griffin Plot[8]

The upper figure is the “Design Curves” of peak amplitude on the Griffin plot. Each curve is related to a constant Reynolds number and shows the effect of Reynolds number on the Griffin Plot. These design curves permit rapid estimation of the peak amplitude for giving the Reynolds number and mass-damping. It should be noticed that in figure (a), the mass-damping is plotted logarithmic, which is different from figure (b). The condition for this plot is that it should be used in the regime at the mass-damping $\alpha < 1.2$.

2) Drag Coefficient

Achenbach and Heinecke (1980)[9] conducted an experiment in the high-pressure wind tunnel to find out the effect of the Reynolds number on the drag coefficient for a cylinder with different surface roughness.

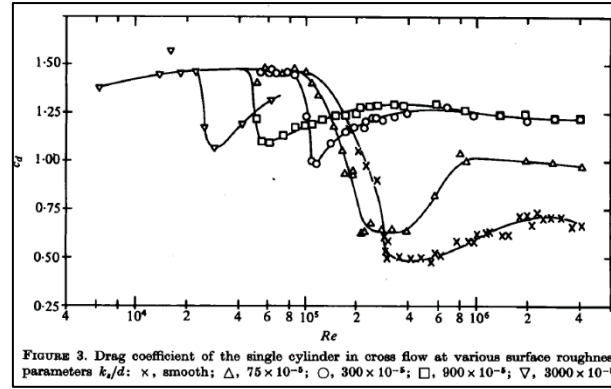


Figure 6 Drag Coefficient for Single Cylinder in Cross Flow at Carious Surface Roughness Parameters[9]

In the plot of the test results, it can be found that different range of Reynolds number and flow range. In the subcritical range, the drag force is close to a constant as the boundary layer is laminar. In the critical flow regime, with the increase of the Reynolds number, the drag coefficient is decreasing. When the drag coefficient reaches the minimum number, the Reynolds number at the minimum point is regarded as the critical Reynolds number. In the supercritical regime, the drag coefficient increases again, and there is no longer intermediate laminar separation for the flow regime. When Reynolds number reaches the trans-critical regime, the drag coefficient is again close to a constant.

Except for the range of Reynolds number, the results also indicate the effect of surface roughness in the experiment. In terms of the drag coefficient, the surface roughness increases the drag coefficient and decreases the critical Reynolds number.

Considering the range of the Reynolds number, the critical Reynolds number for the smooth cylinder is the highest among all the surface roughness conditions. In addition, the increase of the surface roughness will reduce the critical Reynolds number, which will make the minimum drag coefficient appears at a smaller Reynolds number.

2.4. Long Flexible Cylinder

For vertical flexible cylinder test, the experiment from JK Vandiver (2009)[10] shows a large-scaled model test (Miami II) with pipe length of 152.4m and outer diameter of 3.63cm. It is placed in the current with tension in the bottom, which can be seen in the following figure.

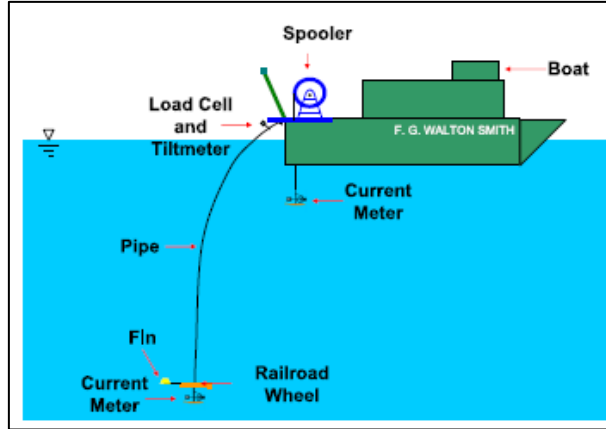


Figure 7 Set-up of Experiment[10]

For a long flexible cylinder, the oscillation differs from each part of the cylinder. The following figure is the measured motion trajectory at each different height.

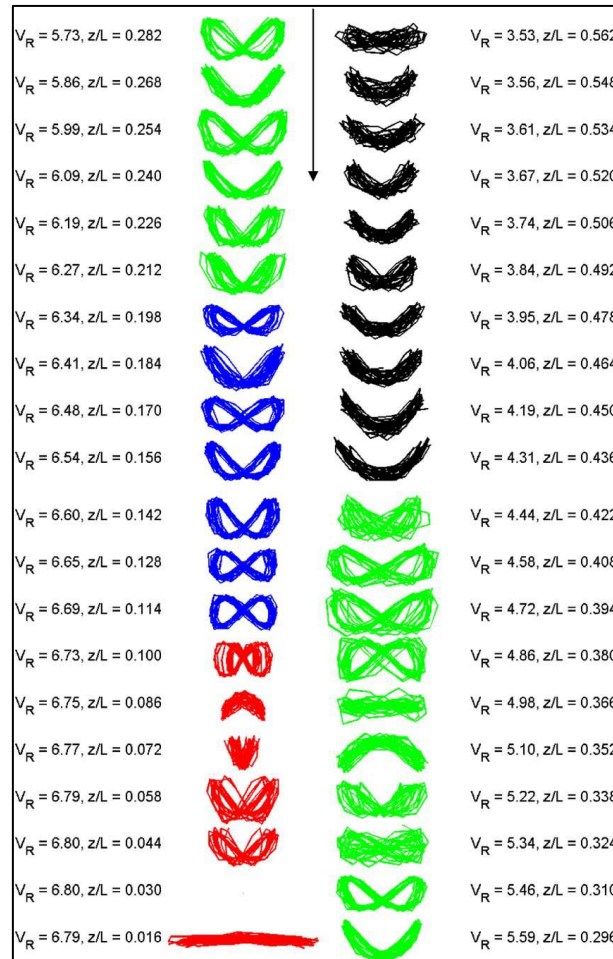


Figure 8 Trajectories of Different Part[10]

From the shape of the trajectories, the region and the phase angel can be found. For example, the black trajectories represent the fourth region, constant crescent shape with 90° phase angel. The green line is the third region, constantly changing trajectories, a region with travelling

waves. And the red one represents the first region, which is the standing wave region.

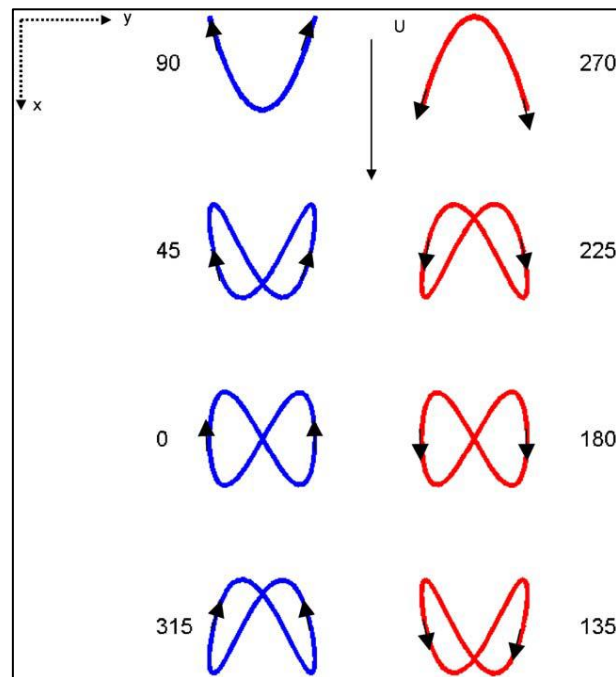


Figure 9 Expression of Phase Angle[10]

To determine the relationship between in-line and cross-flow motion phase angle, the relationship between the trajectories and the phase angle can be found in the upper figure.

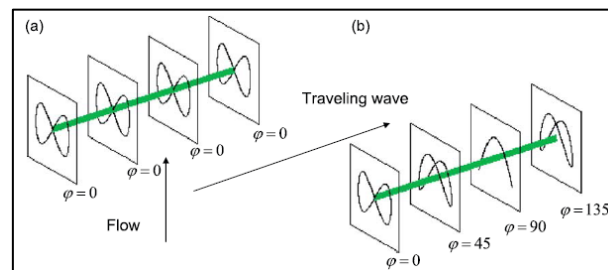


Figure 10 Equal/Different Phase Angles[10]

For short cylinder test, the phase angle remains the same, which is due to the equal cross-flow and inline flow phase speeds. While for the long cylinder, the phase angle for the cross-flow and inline-flow varies, which lead to the change in phase angle and changing trajectories consequently.

2.5. Surface Roughness

From the experiment from Ding (2004)[11], it can be found that both the mean drag coefficient and the amplitude of oscillation are affected by the surface roughness.

The figure of the Base Drag Coefficient has the same meaning of our stationary test as the base drag is considered with four conditions which are the smooth, small roughness, large

roughness and the strakes. The results of the base drag coefficient are in the following figure:

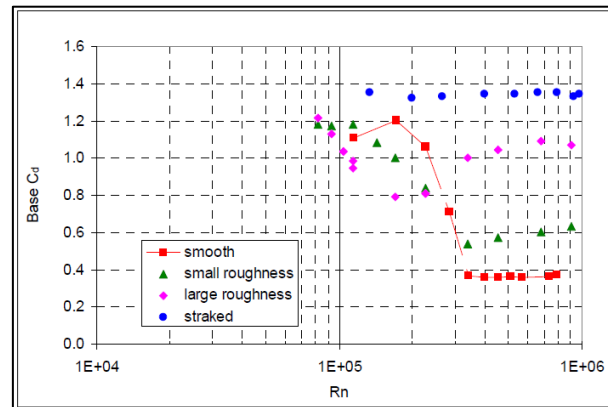


Figure 11 Base Cd vs. Rn for Different Cylinder Models[11]

It can be found that, except for the strakes, the smooth and the rough pipe, at certain Reynolds number, the mean drag coefficient drops quickly. The reason for this phenomenon is mainly because of the transition of the boundary layer from laminar flow to the turbulent flow. While the mean drag coefficient of the strakes is independent on the Reynolds number.

The amplitude of the oscillation is also influenced by the surface roughness of the pipe. The following figure shows the amplitude of oscillation in different reduced velocity with the increase of the surface roughness. The oscillation amplitude of the strakes cylinder is 0 as there is no vibration at all for the strakes cylinder during the free vibration tests.

It can be found that from the figure, the VIV motion is strongly dependent on the surface roughness. For the small roughness and the medium roughness, the amplitude of oscillation tends to be “two peaks” phenomenon, for which the first peak is at $V_{rn} = 4$ to 5, and the second peak is at $V_{rn} = 9$ to 9.

For the rest two conditions, the smooth and the large roughness cylinder, there is only one peak in the amplitude curve. As for the small roughness cylinder, the amplitude is larger than the medium roughness cylinder in all V_{rn} , and the VIV amplitude is larger than the large roughness cylinder in high V_{rn} ($V_{rn} > 8$),

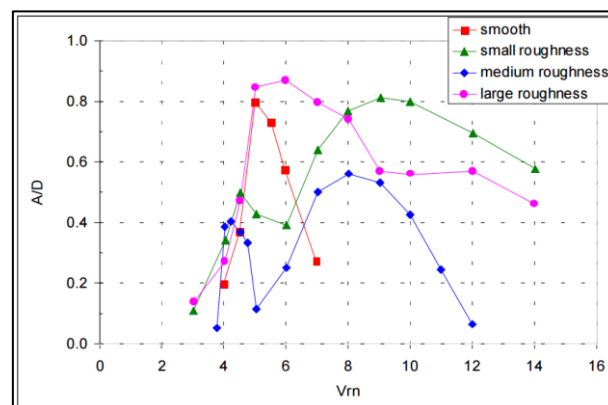


Figure 12 Oscillating Amplitude for Different Surface Roughness[11]

The indication of the observation is that the nature of the cylinder VIV motion is complicated, and it depends on surface roughness and Reynold's number in the critical, flow transition region.

There are two conclusions that should be taken into account: (1) In the critical Reynolds number region, the bare pipe VIV amplitude is sensitive to Reynolds numbers and cylinder surface roughness conditions. (2) In the critical region, cylinders with smooth surface roughness may experience large amplitude motion due to VIV, much greater than it is reported previously.

2.6. Summary of Literature Review

2.6.1. Drag Coefficient

Through the literature review, one can find out the key factor that causes the difference between the large-scaled model test and the small-scaled model test, that is the Reynolds number. One can find that, through the calculating equation of the Reynolds number, the diameter of the oscillator, and the flow speeds of the fluid are the key factors in the calculation. If the fluid used for the flume and the towing tank are both waters at the same temperature, then the viscosity will be the same, which indicates that for the large-scaled model testing in the towing tank, the diameter of the model and the towing speed are higher than the small-scaled model tested in the flume. It will cause the difference in the Reynolds number between these two different scale models with a magnitude of 10 or even higher.

In the study of the relation between the Reynolds number with the potential of the drag coefficient for a cylinder in the stationary test, it can be found that before the flow speed is reaching the critical Reynolds number, there is a tiny increase at the low Reynolds number region. Then the drag coefficient will decrease till the flow speed reaching the critical Reynolds number, in other words, the drag coefficient is the lowest when the flow speed reaches the critical Reynolds number. In the super critical Reynolds number regime, the drag coefficient increases along with the flow speed.

Thus, when testing the drag coefficient for the small-scaled model, the limitation of the flume to achieve high Reynolds number may become the main restriction to the accuracy. If the flow speed of the flume is under the critical Reynolds number, the drag coefficient will decrease only with the increase of the Reynolds number, the minimum of the drag coefficient at the critical Reynolds number and the increase of drag coefficient at the super critical regime will not be observed. In the literature review of the drag coefficient, one may find that the surface roughness may influence the drag coefficient. By increasing the surface roughness, the Reynolds number at the minimum drag coefficient will be reduced.

2.6.2. Oscillation Amplitude

Another important index for the model test is the oscillating amplitude, which will be used as the main reference when evaluating the design of the helical strakes. To evaluate the strake efficiency, one needs to know the maximum oscillating amplitude of the oscillator with and

without the strakes in the free vibration test. In the literature review, the characters that influence the free vibration test are the spring stiffness, the system damping and the mass ratio.

In the free vibration test, the mass ratio of the oscillator is related to the synchronisation regime of the reduced velocity, for an oscillator with lower mass ratio, the synchronisation regime will become wider compared with the higher mass ratio oscillator. If the mass ratio of the oscillator continues to decrease and is lower than the critical mass ratio, then there will be no lock-out to the oscillator during the whole free vibration test.

Comparing the large-scaled model with the small-scaled model, the mass ratio of the large-scaled model is much higher than the small-scaled, which is due to the higher displacement of the large-scaled model and the lower external mass of the oscillator system. For the small-scaled model test, the total mass of the oscillator is much larger than the mass of the cylinder itself, which makes the small-scaled model a higher mass ratio.

In the small-scaled model test, when using the spring, the stiffness of the oscillator is not easy to be controlled in the real testing condition, besides the system damping of the oscillator is another parameter that is hard to change. To solve this situation, the virtual spring-damping system could become a solution as the servo motor can be used for both free vibration test and forced vibration experiment which is another commonly used testing method for the analysis of strake efficiency. However, under the current testing condition, the oscillating amplitude changed with different stiffness or damping can be studied by using the direct numerical solution to build a numerical model and see how the oscillating amplitude will change with different series of stiffness and damping.

3. Set Up of Experiment

For the whole test, when the free vibration test was finished, the test facilities were changed for the stationary test, then repeat the test (first free vibration test and then stationary test) to avoid problems that may not be found in the installation of the facilities. The procedure could be found in the following table:

Table 3 Test List for the Entire Experiment

Test No.	Type of Test	Type of Cylinder
1		Bare Pipe
2	Free Vibration	With Cover
3		With Strakes
4		Bare Pipe
5	Stationary	With Cover
6		With Strakes
7		Bare Pipe
8	Free Vibration	With Cover
9		With Strakes
10		Bare Pipe
11	Stationary	With Cover
12		With Strakes
13		Bare Pipe
14	Free Vibration	With Cover
15		With Strakes
16		Bare Pipe
17	Stationary	With Cover
18		With Strakes
19	Stationary (without cylinder)	\
20	Load Cell Test	\

In each test, before recording the data, the voltage of all the channels should be shifted to zero and make sure the forces, displacement, and the flow speed were set to zero as well.

3.1. Experiment Facilities and Set Up

The test facilities are mainly consisted by the flume, inner and outer frame, load cells, springs, optic laser and data collecting devices.

3.1.1. Flume

To conduct all the experiments, the flume in the Water Lab of TU Delft is used, which is the long tilting flume with a length of 14.3m, width of 0.40m and depth of 0.40m. As for the flume, the maximum discharge rate is 85 L/s.

3.1.2. Load Cell

The supplier of the load cells is SCAIME. For the AL10C3SH5E load cell, the maximum capacity is 10kg, these load cells were used to measure the in-line forces during the free vibration and the stationary test. For the AL30C3SH10E load cells, the maximum capacity is 30kg and this load cell is used to measure the cross-flow force especially for the stationary test. Before the experiments, all the load cells are tested to calculate the scale data in response to the output voltage and measured force as the results of the forces are recorded and stored for further investigation.

Table 4 SCAIME Load Cell Test

Load Cell No.	Output Free	Voltage Output Loaded	Voltage Conversion	Conversion on measurements
Model: AL10C3SH5E				
AL10 314368	0.2607	0.0602	11.8380524	11.97
AL10 314377	0.30836	0.1082	11.858161	12.02
AL10 314397	0.2837	0.4828	11.9212933	11.87
AL10 314380	0.2166	0.01826	11.9669734	11.70
Model: AL30C3SH10E				
AL30 317982	0.2839	0.3516	35.0595199	35.198
Mass for Test				
Mass (kg)	0.24195	Force(N)	2.3735295	

For the free vibration test, the inner frame in this test, which can measure the displacement of the cylinder, is connected to the outer frame through 4 load cells and several springs on top of the inner frame to provide different stiffness.

The load cell arrangement can be found in the following table:

Table 5 Arrangement for Load Cell in Free Vibration Test

Place	Load Cell Number
LR (Left Up)	AL10 314380
RU (Right Up)	AL10 314377
LD (Left Down)	AL10 314397
RD (Right Down)	AL10 314368

In the stationary test, the combination of the load cells was changed on top of the inner frame, the springs were removed, and to connect the inner frame with the outer frame, two load cells would be used.

If we compare the load cell arrangement in the free vibration test with the stationary test, we can find that both the load cell for the left up and the right up were kept. The load cell for the left down was moved to the top of the inner frame to measure top horizontal force, the load cell from the right down was removed and would not be used in stationary test.

As the load cell is used for measuring the top vertical force, the new one with the maximum capacity of 30 kg applied, used considering the total weight of the inner frame, the arrangement of the load cells could be found in the following table (seen from the direction of the water flow):

Table 6 Load Cell Arrangement for Stationary Test

Place	Load Cell Number
TH (Top Horizontal)	AL10 314397
TV (Top Vertical)	AL30 317982
LR (Left Up)	AL10 314380
RU (Right Up)	AL10 314377

The arrangement of the load cells can be seen in the following figure:

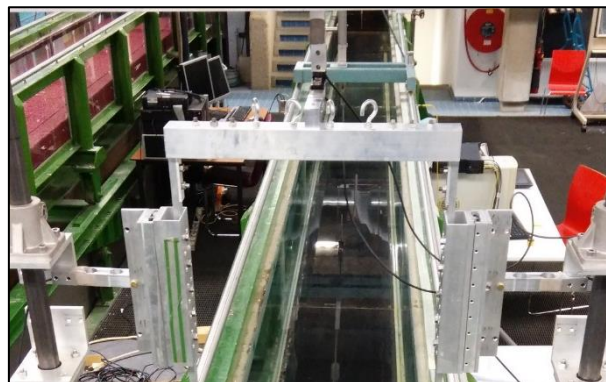


Figure 13 Load Cell Combination for Stationary Experiment

3.1.3. Optic Laser

For the free-vibration tests, the MICRO-EPSILON optic laser ILD1302-200 was used to measure the relative displacement between the inner and outer frames, which equals to the displacement of the cylinder as the cylinder was connected to the inner frame. The available distance for the laser to record is between 6cm and 26cm, thus the maximum oscillation amplitude for the laser to measure is 10cm. The maximum oscillations, as we expected was of the order of 1.2D (5 cm), which was in the range of the measurement by the laser. The optic laser was also tested and calibrated before the experiments.

Table 7 Optic Laser

Item	Description
Supplier	MICRO-EPSILON
Model	ILD1302-200
Minimum Range (cm)	6
Maximum Range (cm)	26

The optic laser is installed on top of the outer frame to measure the displacement of the inner frame which represent the displacement of the cylinder. As the available range for the laser is between 6cm and 26cm, an extra panel was added on top of the inner frame considering that the height of the laser was fixed.



Figure 14 Free Vibration Experiment

3.1.4. Frictionless Table

On each side of the frame, there was a NKL 3.230-KS frictionless table, which was from SCHNEEBERGER for the side roller. The frictionless table has a maximum stroke of 15.5cm, which was larger than the expected maximum oscillation. The original friction on each bearing was too high, which may stop the VIV. To reduce the friction force as less as possible, the slide tables were opened and bolts were loosed, which reduced the friction force to 0.10N on each bearing was achieved, and allowed VIV to occur.

Table 8 Frictionless Table

Item	Description
Supplier	SCHNEEBERGER
Model	NKL 3.230-KS
Maximum Stroke (cm)	15.5
Friction Force (N)	0.10

3.1.5. Frame

The outer frame is set up 8m downstream from the inlet of the flume to ensure that the water flow is steady and will not be influenced neither by the inlet in front nor the panel in the end of the flume.

As the outer frame of the test facility is built on the flume and connected with the flume to make itself steady, it may cause some inaccuracy during the measurement. For example, the vibration from the flume will be transported to the test facility and been recorded as noise in the results.

The natural frequency of inner frame and the outer frame should be higher than the natural frequency of the vortex shedding frequency. In the previous experiment, the natural frequency of the inner frame is 13Hz and the natural frequency of the outer frame is 8Hz. The expected natural frequency for the vortex shedding in the condition of the maximum discharge rate during this experiment is 2.5Hz. The influence of the frame could be neglected according to the differences in natural frequency.

For the stationary test, the springs were removed during the experiment then the cylinder was kept in the middle (20 cm from the bottom) of the flume. Besides, the added weight in the free vibration test was removed, due to the reason that it made some trouble in installing the load cell on top of the inner frame.

3.1.6. Test Model

For the models to be installed, 6 pieces of covers and 6 pieces of strakes were used for the test.

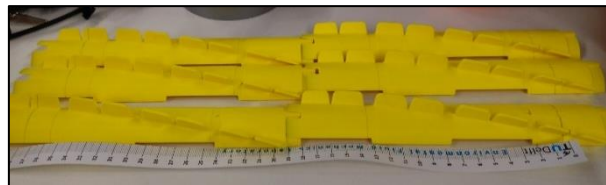


Figure 15 The models before cutting

Each cover and the strake had a length of 24cm, to make the model fitted for the length of the cylinder (37.5cm in length, 4cm in diameter), the models were cut in the carpenter and polished.

In each piece of model, there were two places designed for tiding up, thus, before cutting, these places shall be kept for the tiding up convenient.



Figure 16 Cutting the Cover

After the cutting and polishing, the models were installed on the cylinder and fixed with tape. Considering the actual working condition, there were gaps between the model, thus there is a

2mm gap between each model which can be seen in the following figure.

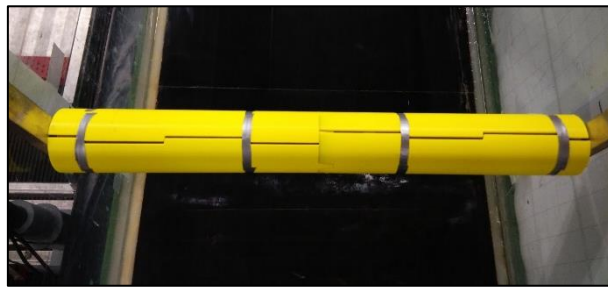


Figure 17 Covers with Cylinder

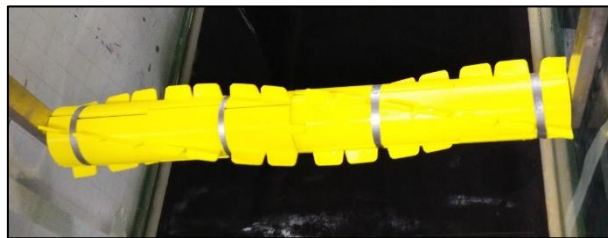


Figure 18 Strakes with Cylinder

After cutting the models, the test was ready and the models could be used for the next procedure.

3.1.7. Free Vibration Model

The natural frequency of the inner frame is determined by the total mass of the inner frame and the total stiffness of the springs. The springs we choose for this experiment are four springs which provided a stiffness of $k=340$ N/m in total. For the inner frame, the total mass is $m=2.550$ kg (added with the slide tables).

To make sure that the natural frequency of the inner frame is close to the frequency of the VIV, during the first experiment, the result is not satisfied as the vibration was too small because of the difference in natural frequency of the frame and the VIV. Thus, the mass of the inner frame was increased by adding additional mass (two pieces of steel bar with a total weight of 2.262 kg), which made the total mass of the inner frame equals to 4.812 kg. Considering the length of the cylinder is 375mm with a diameter of 40mm, the mass ratio of the bare pipe is calculated as $m^* = 10.2$.

3.1.8. Testing Procedure

The cylinder was fixed during the stationary test, thus, the inner frame and the outer frame were connected by load cells.

The procedure for the stationary test is as follows:

- 1) Place the cylinder (frame) at the designed position (20cm from the bottom of the flume);
- 2) Fill the flume with water at the water depth of 40cm, wait until the surface of the water is tranquilized;

- 3) Shift the output voltage of each load cell to zero from the test software;
- 4) Start the water, lower the panel at the end of the flume with the pre-designed height in order to keep the water level at 40cm at the frame;
- 5) When the discharge rate is steady, start to record the data for 3 minutes with a sample collecting rate of 100Hz.
- 6) After recorded one data, lower the panel, increase the discharge rate and repeat the test.

As there was no VIV condition in the stationary test, the step of the discharge rate was chosen as 5L/s, from 30L/s to 60L/s.

3.2. Data Analysis

3.2.1. Data Acquisition

The voltage measured by the loadcell, flow meter and the optic laser, is processed through the amplifier. The voltage signal then comes to the Analogue/Digital converter, which is transferred to readable data for the computer. Then the DASyLab program will process the voltage data into the force, flow speed and displacement through different scale numbers then saved the force data. This step is called the data acquisition step. The typical acquisition and procession are shown in Figure 19, let us take one single load cell for example.

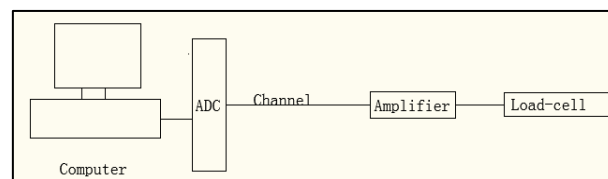


Figure 19 Example of Acquisition and Procession

(1) Amplifier

The amplifier (conditioner) is used to connect the load cell with the ADC (Analogue/Digital Converter) and supply the power to the load cell as well, it is also called as “black box” and it is made by the Water Lab itself.



Figure 20 Amplifier

The amplifier is used in every load cell as well as the optic laser, and it is powered by the dual power supply which will be mentioned later.

(2) Power Supply

The inappropriate power supply to the amplifier can cause inaccuracy in the measurement. The reason for the inaccuracy is that for those power supply like a travel charger, the output of the voltage will be easily affected by other electronic devices, even if they are not in the same socket. The change of the voltage in the output of the power will directly influence the output of the amplifier, and there will be noise in the voltage which will influence the data acquisition.

Thus, the constant-voltage power supply is needed in the experiment to provide a stable voltage without causing noise in the measurement, it is shown in the following figure as the Delta Elektronika E018-0.6D Dual Power Supply.



Figure 21 Delta Elektronika, Dual Power Supply E018-0.6D

The detailed information of the power can be found in the following table:

Table 9 Delta Dual Power

Item	Description
Part Number	E018-0.6D
Manufacturer	Delta Elektronika
Weight	2.70kg
Dimensions	22x18x10 LxWxH (cm)

This power supplies all the amplifier, which turns out to be quite satisfying. Thus, in the future experiment, a dual power supply is strongly recommended to avoid the noise in the measurement.

(3) ADC

ADC is short for Analogue/Digital Converter (A/D Converter), which is used in the measurement to change the analogue results supplied by the amplifier into digital results and then stored by the computer.

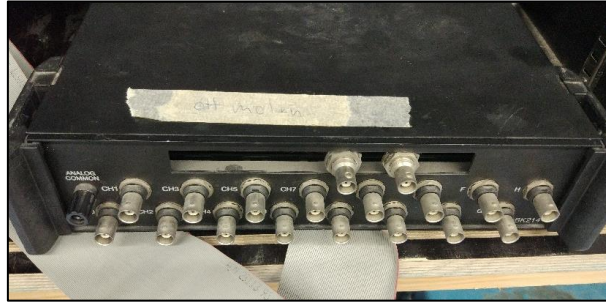


Figure 22 A/D Converter Made by Water Lab

3.2.2. Data Processing

After each force has been processed and stored, the data analysis begins. In the data analysis, for the free vibration test, the idea is to calculate the forces and displacement along with the reduced velocity of the oscillator, and for the stationary test, only the forces along with the Reynolds number are needed.

The list of all the acquired channels and the data matrix for free vibration test is as follows:

Table 10 Channels for Free Vibration Test

Channel	Connected Device	Measured Element
0	Measuring Time	Time (s)
1	Fluid Velocity	Flow Rate In Flume (m/s)
2	Right Down Load Cell	Decomposed Horizontal Force (N)
3	Right Up Load Cell	Decomposed Horizontal Force (N)
4	Left Down Load Cell	Decomposed Horizontal Force (N)
5	Left Up Load Cell	Decomposed Horizontal Force (N)
6	Optic Laser	Displacement of inner frame (m)
7	\	\

```

DASYLab - V 13.00.00
Worksheet name: FreeVibrations_4LC
Recording date   : 1/8/2016, 2:12:22 AM
Block length    : 64
Delta           : 0.01 sec.
Number of channels : 7
Measurement time[s];Velocity [m*Hz];HorizontalForce [N];VerticalDispl
[mm];LoadCell_RD [N];LoadCell_RU [V];LoadCell_LD [V];LoadCell_LU [V];
0.00;0.16017;0.27574;-0.31173;0.66932;-0.37782;0.52453;-0.54029;
0.01;0.15971;0.36647;-0.46432;0.60721;-0.41817;0.54989;-0.37247;
0.02;0.16096;0.45319;-0.48720;0.47936;-0.23842;0.48831;-0.27606;

```

Figure 23 Data matrix for free vibration test

The list of all the acquired channels and the data matrix for the stationary test are shown as follows:

Table 11 Channels for Stationary Test

Channel	Connected Device	Measured Element
0	Measuring Time	Time (s)
1	Fluid Velocity	Flow Rate In Flume (m/s)

2	\	\
3	Right Load Cell	Decomposed Horizontal Force (N)
4	Top Vertical Load Cell	Total Vertical Force (N)
5	Left Load Cell	Decomposed Horizontal Force (N)
6	\	\
7	Top Horizontal Load Cell	Decomposed Horizontal Force (N)

```

DASYLab - V 13.00.00
Worksheet name: StationaryExperimentsWrite
Recording date   : 1/7/2016,  2:06:27 AM
Block length    : 64
Delta           : 0.01 sec.
Number of channels : 5
Measurement time[s];V [V];LC314377 - Right [V];LC317982 - TopV [V];LC314380 -
Left [V];LC314397 - TopH [V];
0.00;2.10974;-0.06409;0.94607;0.22492;-0.26978;
0.01;2.09693;-0.08209;0.94119;0.22279;-0.27589;
0.02;2.08808;-0.06378;0.94333;0.24934;-0.27436;

```

Figure 24 Data Matrix for Stationary Test

All the test data are stored in “.ASC” form and prepared for the processing. The analysis was performed by using a MATLAB program, the MATLAB code was pre-designed and has already been used in former test which proved to be sufficient.

During the data processing, there are several parameters that were given or measured before the processing:

(1) D = Cylinder Diameter

The diameter D for the bare pipe is $D = 0.040m$, while for the cylinder with the cover or the cylinder with the strakes, the diameter D was set to be $D = 0.046m$ instead.

(2) ρ = Fluid Density

The experiments were all performed in the flume and the fluid in the flume was fresh water, which gave a density of the water as $\rho = 1000 \text{ kg/m}^3$.

(3) L = Cylinder Length

The length of the cylinder remains the same as $L = 0.375m$.

(4) $Visc$ = Viscous Flow Coefficient

The kinematic viscous flow coefficient was given as $Visc = 1.15 \times 10^{-6}$.

3.2.3. Stationary Test

For the stationary test, the stored force data matrix contains 7 columns and the length is defined by the time in the measurement. For example, in the two minutes' measuring $T = 2 \text{ min}$, the step is chosen as $\Delta t = 0.01 \text{ sec}$, then the length of the lines is calculated as $N = T/\Delta t = 12000$. The Nyquist frequency $f_{Nyquist} = 1/(2\Delta t) = 50\text{Hz}$. The numbered channels are 0-time, 1-flow velocity, 2-total horizontal force, the 4-horizontal force measured by the load cell, 5-horizontal force measured by the left load cell, 6-horizontal force measured by the top loadcell.

In the stationary experiment, four coefficients are calculated, which are the mean drag coefficient, the oscillation drag coefficient, the oscillation lift coefficient and the Strouhal number.

The calculation of these coefficients is shown in the following steps:

(1) Re = Reynolds Number

The Reynolds number will be used as the X-axis for the rest four coefficients in evaluating the stationary test which explains the flow speed in the test.

$$Re = \frac{V * D}{Visc} \quad \text{Equation 4}$$

Here, V is the flow speed in the flume (m/s), which is calculated by the mean value of the flow velocity. The flow velocity measured by the flowmeter placed upstream of the cylinder in the same water depth.

(2) MeanDrag = coefficient of the mean drag force (Horizontal Direction)

The mean drag coefficient is calculated by using the mean value of the total horizontal force, which is the column number 2 in the force data matrix, which is symbolled as *FxMean*. For each test with different discharge rate, the *FxMean* is calculated with the different force data matrix. The mean drag coefficient is calculated as the following equation.

$$\text{MeanDrag} = \frac{FxMean}{\frac{1}{2} \rho * D * L * V^2} \quad \text{Equation 5}$$

(3) OscDrag = coefficient of the Oscillation drag force (Horizontal Direction)

$$\text{OscDrag} = \frac{FxOsc}{\frac{1}{2} \rho * D * L * V^2} \quad \text{Equation 6}$$

The horizontal oscillation force *FxOsc* is the standard deviation of the difference between the horizontal force and the averaged horizontal force.

(4) St = Strouhal Number

To calculate the Strouhal number, one needs to get the vortex shedding frequency, which is calculated by the function of "Frequency Content". The function of frequency content is to determine the frequency range first, which is from 0Hz to the half of the highest frequency. The half of the highest frequency is denoted as the Nyquist frequency. Then, Fast Fourier Transform (FFT) is applied to each column. The selected results are the first half of the results denoted from FFT due to the Nyquist frequency.

After the force results are processed with FFT, the absolute value of the results are saved and the maximum figure is chosen as the index of the frequency processed by the FFT. Then this frequency is also denoted as the vortex shedding frequency, which is used to calculate the Strouhal number later.

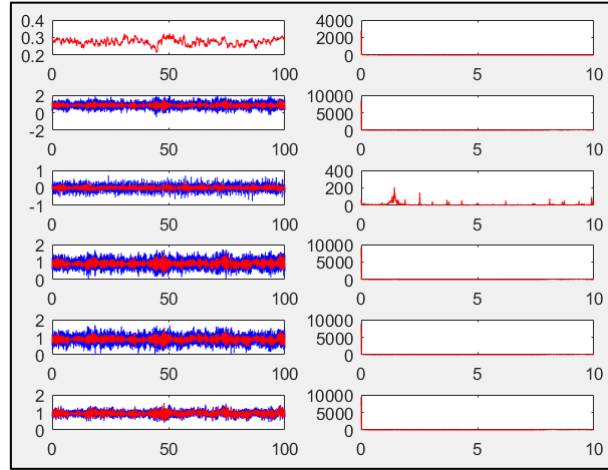


Figure 25 FFT results for one test at Q_400_Forces with Frequency Filter 10Hz

In the figure, the maximum or the index of the oscillating frequency is shown in the third line, and the frequency is estimated to be around 1 to 2Hz, which is saved as the “*VortesShedFreq*” and is used for calculating the Strouhal number *St*.

$$St = \frac{VortesShedFreq * D}{V} \quad \text{Equation 7}$$

(5) *OscLift* = coefficient of the Oscillation lift force (Vertical Direction)

The vertical oscillation force *FyOsc* is calculated by the standard deviation of the difference between the value of the vertical force and the mean value of the vertical force. The coefficient of the Oscillation lift force is calculated as

$$OscLift = \frac{FyOsc}{\frac{1}{2} \rho * D * L * V^2} \quad \text{Equation 8}$$

3.2.4. Free Vibration Test

At the beginning of the free vibration test, two tests were done to get the natural frequency of the oscillator in the air and in the water, these tests were the free vibration in the air (Dry Test) and the free vibration in the water (Wet Test).

For the free vibration test, the recorded force and displacement data matrix is made by 7 columns, which are: 1-velocity, 2-calculated horizontal force, 3-vertical displacement, 4-load cell at right down position of the frame, 5- load cell at right up position of the frame, 6- load cell at left down of the frame, 7-load cell at left up of the frame.

In the free vibration test, four characters are shown in the plotted result, which are the amplitude of oscillation, the frequency of oscillation, the mean drag coefficient and the oscillation drag coefficient. And the processing method of each characters will be introduced one by one.

In the test, there are five factors that we are interested in, these factors will be shown in the test results for evaluation at the next chapter. The factors are:

- Oscillation Amplitude;
- Oscillation Frequency;
- Mean Drag Force in Horizontal Direction;
- Oscillation Drag Force in Horizontal Direction;
- Relative Flow Rate.

The calculation of these coefficients is shown in the following steps:

(1) V_r = reduced velocity

In the free vibration test, the x-axis is defined by the reduced velocity, which is expressed by the symbol of V_r . The velocity used to calculate the reduced velocity for each results matrix is the mean value measured by the flow meter, and the natural frequency of the oscillator in the water is measured each time during the calibration.

The relative velocity is used for the estimation as the X-axis, which is calculated as:

$$V_r = \frac{V}{NatFreqWet * D} \quad \text{Equation 9}$$

The $NatFreqWet$ means the natural frequency calculated in the free vibration for the cylinder in the water.

(2) $OscFreq$ = Oscillation frequency

When processing the force matrix, the first is to process Fast Fourier Transform (FFT) on all the columns, the results are shown in the following figure:

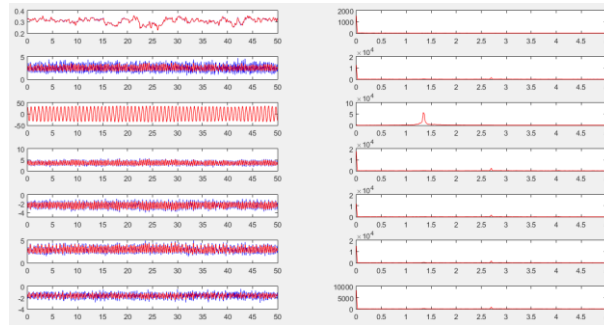


Figure 26 FFT result for Q_455_Force with Frequency Content at 5Hz

In the figure, the third line is the result after FFT, the left column is the measured force or displacement versus time, the right column is the FFT results. Taking the third row for example, the maximum FFT results lies at approximate 1.35 Hz, which is then defined as the index or the max of the frequency, and it is used for the calculation of the oscillation frequency.

(3) $OscAmp$ = coefficient of the Oscillation amplitude

The Oscillation amplitude was used to evaluate the performance of the cylinder in VIV, which was calculated as

$$OscAmp = \frac{\sqrt{2}\sigma_{Displ}}{D * 1000} \quad \text{Equation 10}$$

The standard deviation of the displacement used in calculating the oscillation amplitude is the same definition of the coefficient as the OCEANIC test results.

(4) *MeanDrag* = coefficient of the mean drag force in the horizontal direction

To get the mean drag force, the *FxMean* was needed by calculating the mean value of the horizontal force *Fx*.

$$\text{MeanDrag} = \frac{FxMean}{\frac{1}{2}\rho * D * L * V^2} \quad \text{Equation 11}$$

(5) *OscDrag* = coefficient of the Oscillation drag force in horizontal direction

To calculate the oscillating drag coefficient, one need to calculate the oscillating horizontal force first, which is denoted as *FxOsc*. The *FxOsc* is the standard deviation of the difference between the measured total horizontal force and the mean value of the total horizontal force, which is calculated as $FxOsc = \text{std}(Fx - FxMean)$. Then the oscillating drag coefficient is calculated as:

$$\text{OscDrag} = \frac{FxOsc}{\frac{1}{2}\rho * D * L * V^2} \quad \text{Equation 12}$$

3.3. Stationary Test Results

The test results are shown in the following figure, to identify the different type of cylinder, we use a blue line for the bare pipe test, a red line for the pipe with cover and black line for the pipe with strakes.

In the figure, there is a shift for the cover and the strakes as the diameter increased from 0.04m to 0.046m, thus the Re is larger than that of the bare pipe test at the same discharge rate.

3.3.1. Mean Drag Coefficient

The mean drag coefficient could be used to estimate the mean value of the drag force in the test, in the figure we can see that when comparing to the Bare Pipe, there is approximately 50% increasing in the Pipe + Strakes. Thus, the strakes do increase 50% of the mean drag force in the test.

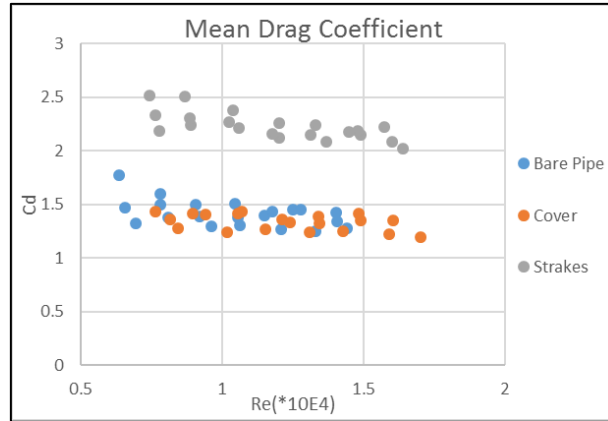


Figure 27 Main Drag Coefficient for Stationary Test

3.3.2. Oscillation Drag Coefficient

For the Oscillation drag coefficient, the difference is small, the Bare Pipe and the Bare Pipe + Cover are almost the same, and the results for the Bare Pipe + Strakes is higher than the rest two conditions at a range of $Re = 0.9 \times 10^4 \sim 1.3 \times 10^4$, with an increase of 10%, except for this range, the Oscillation drag coefficient is similar.

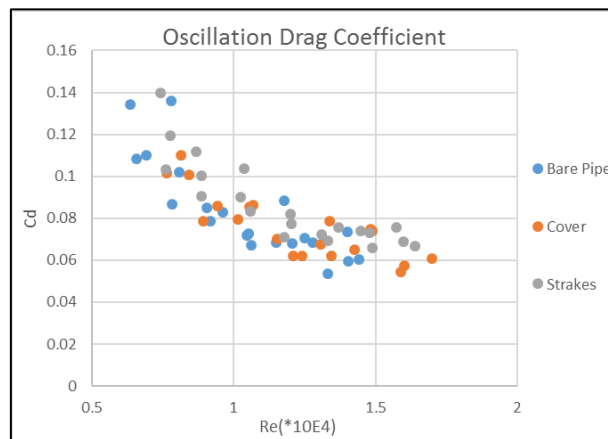


Figure 28 Oscillation Drag Coefficient for Stationary Test

3.3.3. Oscillation Lift Coefficient

For the oscillation lift coefficient, we can find that the Bare Pipe with Cover is the highest (30% higher than the Bare Pipe) which means the highest vortex force around the cylinder. This is because of the larger diameter compared to the Bare Pipe.

As for the Bare Pipe with Strakes, the Oscillation drag force is the highest among all the three conditions, 20% less than that of the Bare Pipe test, which means that the strakes can reduce the oscillation force when is perpendicular to the flow direction.

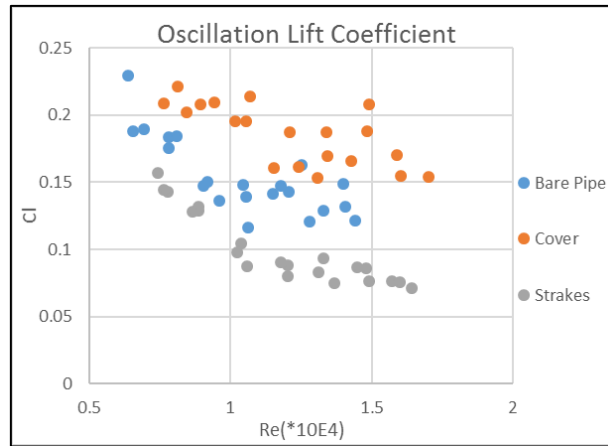


Figure 29 Oscillation Lift Coefficient for Stationary Test

3.3.4. Strouhal Number

The Strouhal number is used to describe the oscillating flow mechanisms. For large Strouhal numbers (order of 1), viscosity dominates fluid flow, resulting in a collective oscillating movement of the fluid “plug”.

In the Strouhal number of the strake model, some dots are far beyond the normal value, which is abnormal. For the other conditions, we can see that the strakes cause the turbulence flow and have the higher St number. While for the Bare Pipe + Cover, the St number remains to be around 0.2 for all the Re conditions.

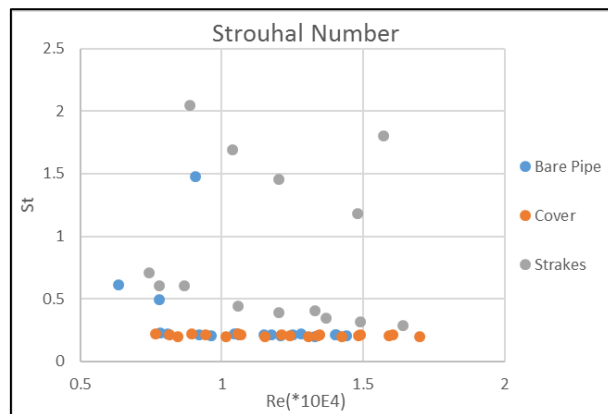


Figure 30 Strouhal Number for Stationary Test

3.4. Free Vibration Test Results

For the free vibration test, which is the best way to show how the strakes can decrease the VIV. In the free vibration test, we can get the natural frequency of the vibration of the cylinder in the water by giving the cylinder an initial displacement and then measure the oscillating frequency, the test results are as follows:

Table 12 Natural Frequency of Models in Water

Bare Pipe	NatFreqWet (Hz)
Test 1	1.3105
Test 2	1.3419
Test 3	1.3320
With Cover	NatFreqWet (Hz)
Test 1	1.3068
Test 2	1.2658
Test 3	1.2601
With Strakes	NatFreqWet (Hz)
Test 1	1.2662
Test 2	1.2620
Test 3	1.1719

3.4.1. Amplitude of Oscillation

In the free vibration test, the oscillation amplitude of the Bare Pipe and the Cover have almost the same figure except for the shift in the x direction as the cover has a larger diameter increases the Reynolds number. The highest amplitude of bare pipe lies at the point (5.763, 0.894), which gives the highest amplitude of oscillation equals to 0.894.

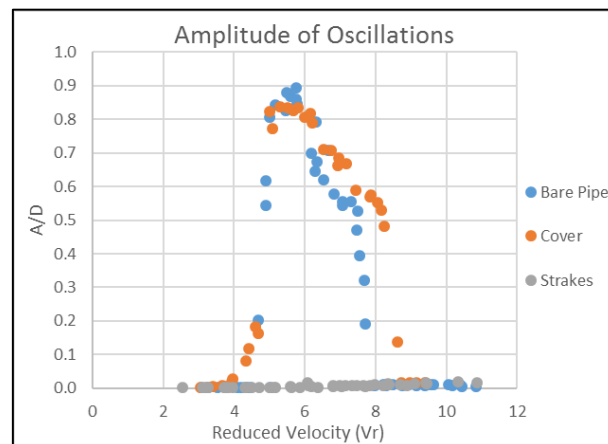


Figure 31 Amplitude of Oscillations for Free Vibration Test

For the Strakes, the amplitudes are close to zero when plotted with other two models, it would be better to show the result along and the amplitude of oscillation is shown in the following figure. And it can be found that the highest amplitude of strakes is 0.020, which will be used to evaluate the efficiency of the strakes.

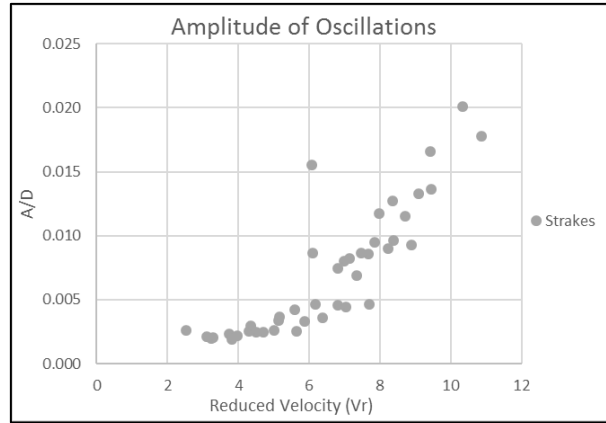


Figure 32 Oscillation Amplitude of Small-scaled Strake Model

The amplitude of oscillation is used to evaluate the efficiency of strakes, which will be discussed in the comparison with the full-scaled test.

3.4.2. Frequency of Oscillation

In the results of the oscillation frequency, there are mainly two groups of frequencies. One is close to the natural frequency of the oscillator (close to 1), the other one increases with the reduced velocity.

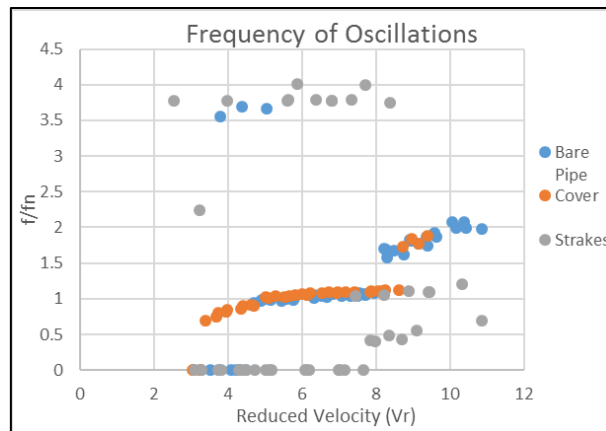


Figure 33 Oscillation Frequency for Free Vibration Test

Not all the frequencies are shown in the figure as some frequencies can be $f = 35f_N$ in the figure, which is too far from the mean data.

3.4.3. Mean Drag Coefficient

In the mean drag force, as we all know, the strakes will increase the drag force of the cylinder, while in the test which the Vr number in the middle range ($Vr = 5 \sim 7$), the mean drag force of the strakes is the lowest. For the Bare Pipe + Cover, the mean drag force is higher than the Bare Pipe as the increase of the diameter.

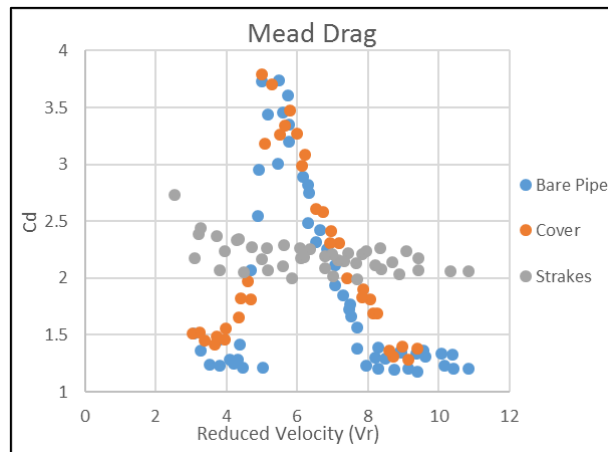


Figure 34 Mean Drag for Free Vibration Test

3.4.4. Oscillation Drag Coefficient

In the oscillating drag force, for the bare pipe and the cover, the oscillation drag are both the bell shape curve, while for the strakes, due to the suppression effect, the oscillating drag coefficients are controlled in a low range. There is no bell shape curve of the oscillating drag force for the stake model, and the drag coefficient continues dropping with the increase of the reduced velocity.

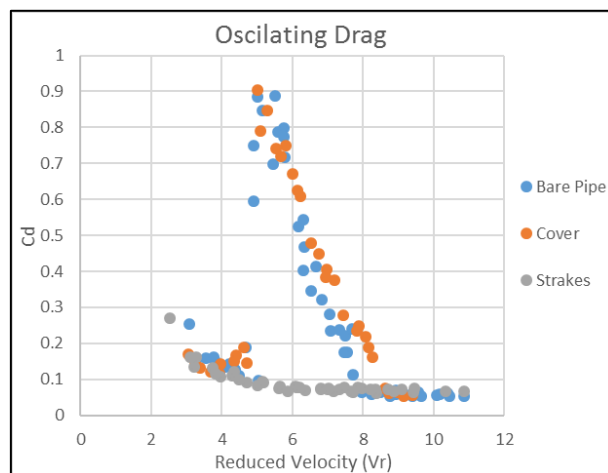


Figure 35 Oscillation Drag for Free Vibration Test

4. Comparison and analysis

In this chapter, to find out the difference between the full-scaled model test by the towing tank and the small-scaled test from the flume, the full-scaled mode test offered by Lankhorst will be compared with the small-scaled mode test from the water lab.

The further analysis will focus on the reason of causing the difference between the full-scaled model and the small-scaled model, as well as the difference between the flume and the towing tank.

4.1. MARIN

4.1.1. Introduction of MARIN's test

In the test from MARIN, there are three types of tests, which are the vertical oscillation in still water (KC test), the non-oscillating tow test (Drag test) and the vertical oscillation while towing (VIV test).

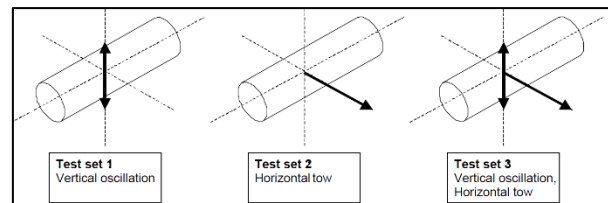


Figure 36 Types of Test

In the experiment, the bare pipe model has an outer diameter of 324mm, with 100 microns (0.1mm) Carborundum roughness on the bare pipe, which gives a relative roughness of $k/D=0.0003$. There are 11 different models in total for the MARIN's test, the detail of the models are as follows:

Table 13 Total Test Model from MARIN

No.	Model
Bare	324 mm bare Pipe
LH_0	77 mm strakes with corrosion recesses
LH_1	77 mm strakes without corrosion recesses
LH_2	Mat with holes
LH_3	Small wedge type strakes
LH_4	54 mm strakes with corrosion recesses
LH_5	Inverse strakes
LH_6	45 mm strake without corrosion recesses
LH_7	36 mm strake without corrosion recesses
LH_8	54 mm strake without corrosion recesses
LH_9	54 mm strake with openings

For each model, all the three types of test as the Drag test, the VIV test and the KC test were

performed. The different test number indicates different simulation for the strake height, damage and corrosion.

4.1.2. Selection

Among the three types of tests from MARIN, to compare the test with the small-scaled test, the test set 2 “Horizontal tow”, which is the non-oscillating tow test (Drag Test), is the ideal type to indicate the drag coefficient changes with the Reynolds number.

From the MARIN's test results, to compare the full-scaled test with the small-scaled test, the 324mm bare pipe, the LH_1 77mm strake without corrosion recesses are the suitable models for the full-scaled test. In the test of LH_1, the model consists of 324mm diameter of the bare pipe, 2*17mm mat height and 77mm vane height. The results of these two tests can be found in the appendixes of the MARIN's report.

4.1.3. Comparison

As there is no forced vibration test in our test, we only compare the non-oscillating test and focus on the C_d the drag coefficient. Thus, the results of the mean drag coefficient with blockage correction are chosen for comparison.

In the following chart, the bare pipe test is the lowest line (Bare F, Bare B), while the strakes are used in the highest line in the chart.

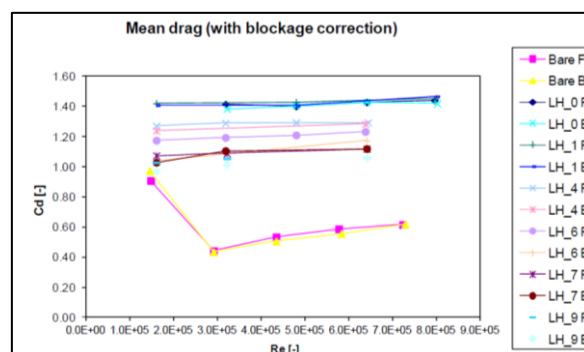


Figure 37 Original Results from MARIN

From the bare pipe test result of MARIN (Bare F, Bare B), we may find that between $Re=1.0E+05 \sim 3.0E+05$, the mean drag is decreasing, and when $Re > 3.0E+05$, C_d increases with the Reynolds number. The average number of the mean drag coefficient in the bare pipe test is 0.6.

For the test with strakes (LH_1 F, LH_1 B), the mean drag coefficient is more stable than that of the bare pipe, there is only a slight increase of C_d and the average result is 1.45. When compared with the bare pipe test, it is found that if strakes are added to the pipe, there will be 140% increase than that of the bare pipe for the mean drag coefficient.

To make it easier for comparison, the test results for the Bare Pipe and the strakes LH_0 are picked out. The data and the figure are in the following:

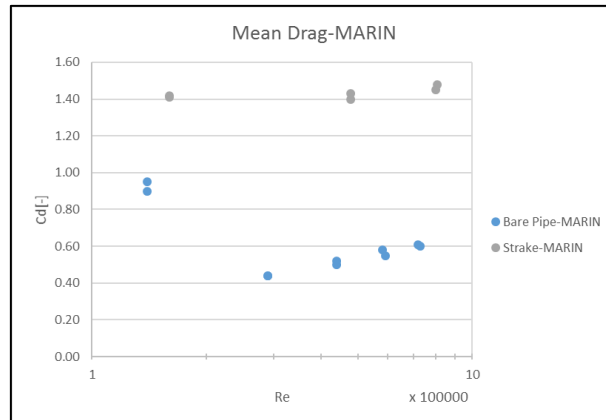


Figure 38 Selected Results for Bare Pipe and Strakes

Table 14 Test Results for Bare Pipe and Strakes

Test No.	Re[E+05]	Cd
Bare F	1.4	0.90
	2.9	0.44
	4.4	0.52
	5.8	0.58
	7.2	0.61
Bare B	1.4	0.95
	2.9	0.44
	4.4	0.50
	5.9	0.55
	7.3	0.60
LH_1 F	1.6	1.42
	4.8	1.43
	8	1.45
LH_1 B	1.6	1.41
	4.8	1.40
	8.1	1.48

When compared with the data that we got, the test is performed in a condition of lower Reynolds number, which is between $Re = 6.0E + 03$ and $Re = 1.6E + 05$. The test results can be seen in the following figure.

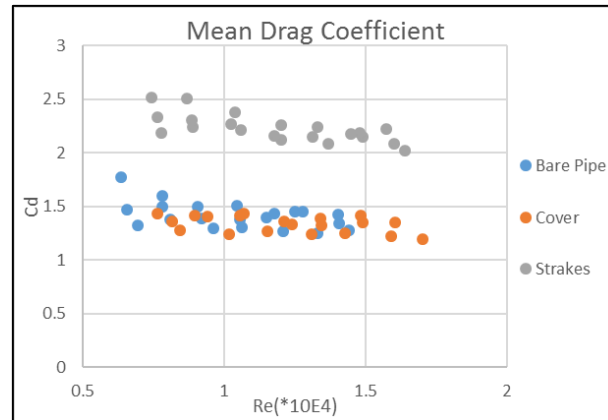


Figure 39 Test Results from Water Lab

For the test result from the MARIN and the data from the Water Lab, if we merged them together we may find the following figure:

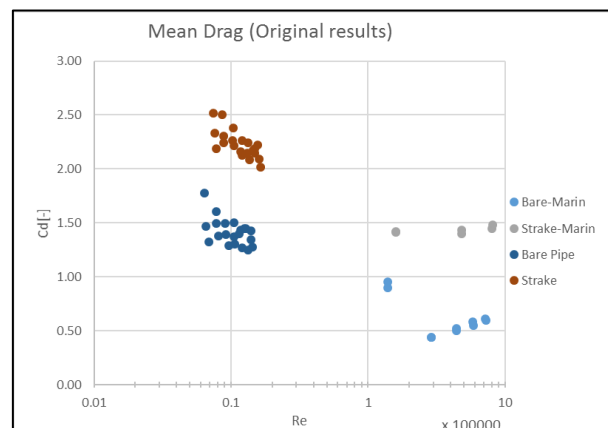


Figure 40 Merged Test Result

In the figure, the mean drag coefficient for the small model test is higher than the large model, which is mainly due to the difference of the Reynolds Number (Low Reynolds Number for the small-scaled model test and high Reynold's Number for the large model).

4.1.4. Blockage Correction

In the experiment from Marine, blockage correction is used in evaluating the drag coefficient of the full-scaled model test, considering the cylinder diameter chosen in the experiment is a little large which might have been desirable from the point of view of blockage.

The blockage correction is originally used in wind tunnel by Allen & Vincenti (1944), then Roshko (1961) use this theory to correct the wall interface effects for the values of velocity and the drag coefficient for the experiment in a wind tunnel with the diameter of the tested cylinder $d=457\text{mm}$ (1.5ft), and the tunnel breadth $h=3352.8\text{mm}$ (11ft), which gives a blockage ratio $d/h=0.136$. The corrected drag coefficient C_d in terms of the measured value C_d' is shown in the following equation:

$$\frac{C_d}{C_d'} = 1 + \frac{1}{2} C_d' \left(\frac{d}{h} \right) - 2.5 \left(\frac{d}{h} \right)^2 \quad \text{Equation 13}$$

The above equation for the blockage correction of the drag coefficient is used in the full-scaled test by MARIN. In the full-scaled test, the diameter with strakes is $d=435\text{mm}$, the cylinder diameter without strakes is $d=324\text{mm}$, the water depth is $h=3800\text{mm}$, the blockage ratio for the strakes is then calculated as $d/h=0.11$ while for the bare pipe $d/h=0.085$.

As the correction equation is a binary linear equation, through the corrected results of the full-scaled test, the original drag coefficient without blockage correction can be calculated and are shown in the following figure:

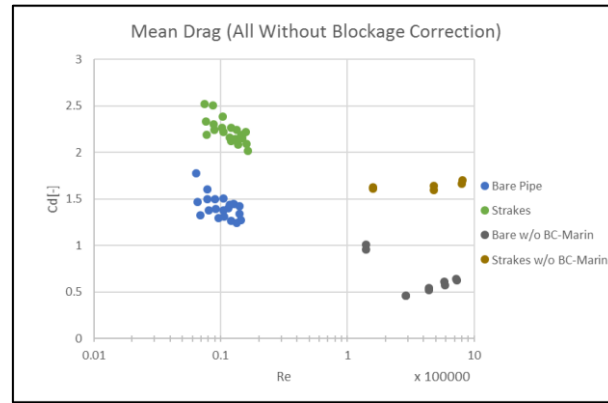


Figure 41 Mean Drag Coefficient Uncorrected

For the small-scaled test, without the blockage correction, the drag coefficients for bare pipe and the cylinder is much higher than the full-scaled test which has been corrected with the blockage correction. The plot of the small-scaled test without blockage correction and the full-scaled test with blockage correction are shown in the following figure:

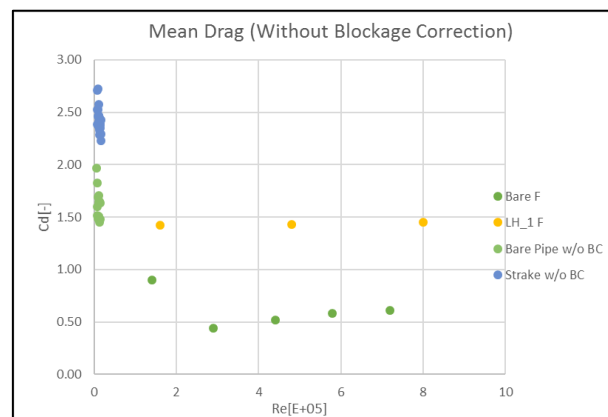


Figure 42 Mean Drag with Uncorrected Small-scaled Results

Using the blockage correction function for the small-scaled test results, the diameter of the bare pipe and the strakes are 40mm and 46mm separately. The water depth is $h=200\text{mm}$, which gives the blockage ratio $d/h=0.20$ for bare pipe and $d/h=0.23$ for the strakes. Then the drag coefficient with blockage correction are shown in the following figure:

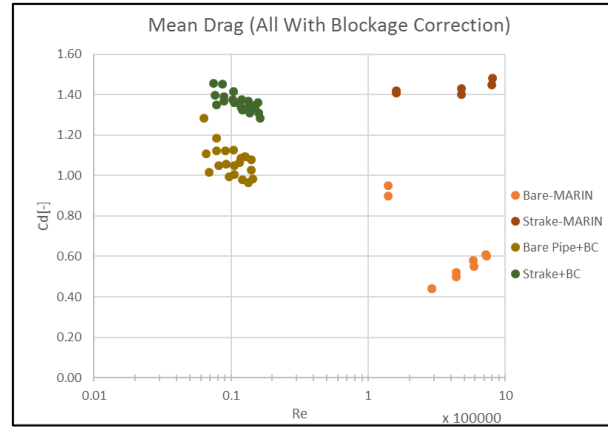


Figure 43 Mean Drag Coefficient with Blockage Correction

In the upper figure, with the blockage correction for the small-scaled mode test, the drag coefficient for the strakes is almost the same with the full-scaled test. While for the bare pipe, the drag coefficient is still higher compared to the full-scaled test. Through the literature study, we know that the difference between the upon drag coefficient is mainly caused by the Reynolds number.

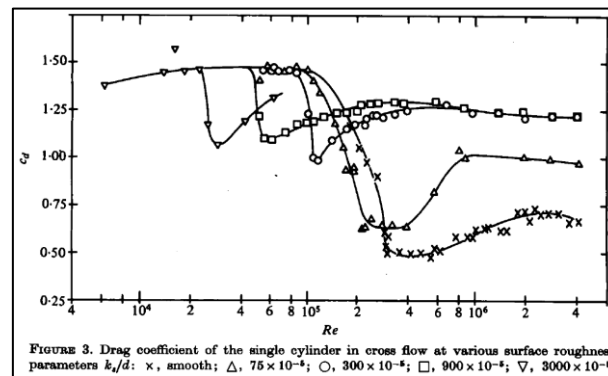


Figure 44 Drag Coefficient of Single Cylinder at Various Roughness [9]

The plot of the “LH_1F” is similar to the smooth cylinder condition in the upper figure which shows a decrease in Reynolds number between 1×10^5 with 3×10^5 which is the subcritical regime and then increase at $Re > 3 \times 10^5$ which is the supercritical regime. The critical Reynolds number is close to $Re = 3 \times 10^5$. For the full-scaled mode test, the lowest drag coefficient is $Cd = 0.43$ at the Reynolds number $Re = 3 \times 10^5$.

For the small-scaled model test of the bare pipe, the Reynolds number is at the subcritical regime, and there is a slight decrease of the drag coefficient with the increase of the Reynolds number.

While for the strake test, both the small-scaled model and the full-scaled model test results are nearly constant, which is due to the change of the water flow by the strakes. Thus, the effect of the Reynolds number cannot be observed.

4.1.5. Evaluation of Blockage Correction

The reason for using the blockage correction, as explained by MARIN, is “because of using the full-scaled strakes, the cylinder diameter chosen was a little larger than might have been desirable from the point of view of blockage”, which is originally from the research by Roshko (1961)[12]. In the full-scaled model test, the diameter of the cylinder is $D_3 = 435 \text{ mm}$ (77 mm strake height) in a water depth of 3800 mm, which gives the blockage ratio as $d/h = 0.11$. Where d is the diameter of the test model, h is the water depth between the surface and the model. To correct the wall interference effects, MARIN uses the following formula as proposed by Allen & Vincenti (1944)[13] in Roshko (1961)[12]:

$$\frac{V}{V'} = 1 + \frac{1}{4} C_d' \left(\frac{d}{h} \right) + 0.82 \left(\frac{d}{h} \right)^2 \quad \text{Equation 14}$$

$$\frac{C_d}{C_d'} = 1 + \frac{1}{2} C_d' \left(\frac{d}{h} \right) - 2.5 \left(\frac{d}{h} \right)^2$$

In the full-scaled model test by MARIN, the blockage correction is used only in the calculation of the drag coefficient. By comparing the values before and after the correction, the drag coefficient is reduced while the velocity is increased.

From the point of view by Allen & Vincenti (1944) [13], the interference between the wake and the tunnel walls gives rise at the position of the model to a velocity increment and a velocity gradient which are not present in an unlimited stream. Further, as required by Bernoulli's equation, the velocity gradient is accompanied by a longitudinal pressure gradient which likewise would not exist in the free air.

The reason for introducing the blockage correction in the experiment is due to the wall interference correction, as is claimed by Roshko (1961) [12], in the wind tunnel experiment for cylinders, to obtain the highest possible Reynolds number. The chosen cylinder diameter was a little larger than might have been desirable from the point of view of the wall interference. The blockage correction is often used in the wind tunnel, while less common for the flume and the towing tank.

Since the blockage correction equation is a quadratic equation, the drag coefficient before correction can be calculated and the below figure shows the effect of the correction for both small-scaled model and the full-scaled model test.

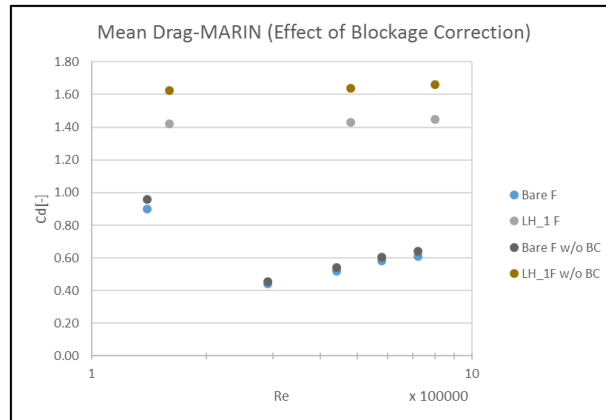


Figure 45 Effect of Blockage Correction for Large-scaled Model

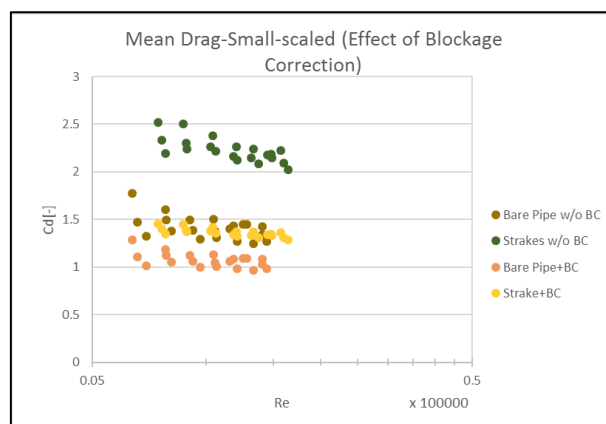


Figure 46 Effect of Blockage Correction for Small-scaled Model

From the Figure 45 and Figure 46 one may find that the blockage correction has a larger effect on the small-scaled model, which is mainly because of the higher blockage ratio d/h as well as the original drag coefficient. In MARIN's experiment, the blockage correction reduced the drag coefficient by 4.8% for bare pipe and 8.7% for the strake model, while in the small-scaled model test, the blockage correction reduced the drag coefficient by 26% for the bare pipe and 35% for the strake model.

In another full-scaled model test by OCEANIC, no blockage correction is used for either the drag coefficient or the velocity. Considering the original purpose of the blockage correction (for wind tunnel to achieve ideal Reynolds number), quite small amount of towing test or the fume test have been considered for blockage correction. Thus, the blockage correction is not recommended for the future model test.

4.2. OCEANIC

4.2.1. Introduction of OCEANIC Experiment

The experiment is conducted in the 200-meter towing tank for Ocean Technology in St. John's Newfoundland, Canada. The towing tank is 12m wide by 7m deep, with a maximum towing

speed of 10 m/s and a maximum towing force of 20kN for the carriage. The basic test model is an aluminium pipe with 6.328m long by 0.325m diameter ($L/D=19.5$), giving the mass ratio of the vibration system as 1.56.

For the bare pipe experiment, the aluminium pipe was covered with a fiberglass jacket which was coated with sand to produce a rough skin for the pipe. The relative roughness of the bare pipe model was $k/D = 0.003$.

For the strake experiment, the bare pipe was covered with a wooden framework and increased the diameter to 0.483m, then applied the strake and the diameter was increased to a reference diameter of 0.511m. The strake fin (vane) height was 0.102m, which is 21% of the model outer diameter.

4.2.2. Mean Drag Coefficient

In the fixed mode test from OCEANIC, the Reynolds number for this test range is from $1.00E + 05$ to $1.20E + 06$, the drag coefficient for the strakes is 1.35 in average, and for the rough bare pipe the result turns to be 1.05 in average.

From the figure below, for the 16D triple helix strake, the drag coefficient is more stable than the rough bare pipe. And for the rough bare pipe, compared with the bare pipe, the increase of the surface roughness reduces the critical Reynolds number and the supercritical Reynolds number. The increasing part of the drag coefficient is due to the supercritical regime of the Reynolds number, however, in the figure the decreasing part and the minimum number of the drag coefficient are not observed in the figure, this is because of the absence of the subcritical and the critical Reynolds number regime.

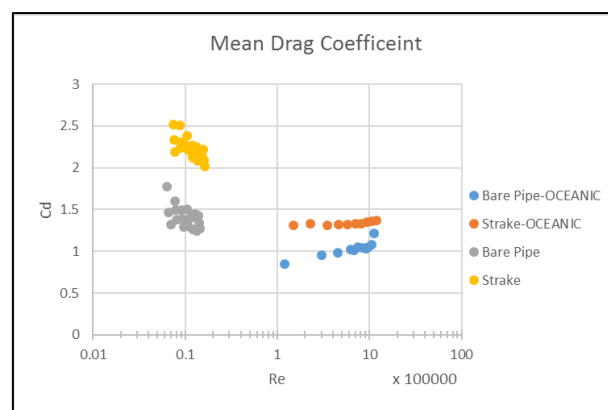


Figure 47 Mean Drag Coefficient-OCEANIC

Combining the drag coefficient results of the full-scaled test the small-scaled test, without the blockage correction of the small-scaled model test, the drag coefficient for the small-scaled strakes is almost twice of the full-scaled strakes. For the small-scaled bare pipe, the drag coefficient is higher than the full-scaled rough bare pipe. The results of the small-scaled and the full-scaled tests are shown in the following figure:

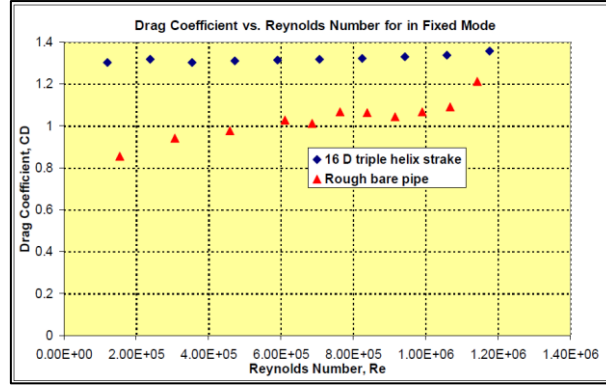


Figure 48 Merged Drag Coefficient without Blockage Correction

The drag coefficient for the small-scaled strake are very close to the full-scaled strake. While for the bare pipe test, due to the influence of Reynolds number in the subcritical regime on the drag coefficient, the small-scaled model has a higher drag coefficient than the full-scaled test. Besides, as the rough bare pipe is chosen for the full-scaled model, the Reynolds number is at the super critical regime, which is the reason why there is an increase of the drag coefficient.

4.2.3. Amplitude of Vibration

In the result from the OCEANIC, the coefficient for the oscillation amplitude is the amplitude ratio A^* , which is defined as:

$$A^* = \frac{\sqrt{2} * \sigma_{Motion}}{D_{cylinder} + 2 * t_{Strake}} \quad \text{Equation 15}$$

Thus, for the full-scaled test, the amplitude of oscillation is defined by using the standard deviation of the motion (displacement of the oscillator). Thus, to compare the experiments, for the small-scaled model test, the amplitude is also achieved by using the standard deviation.

Considering the different scale of the test results between the bare pipe and the stakes, to express the results clearly, it is better to plot the amplitude of oscillation separately. The results from the OCEANIC free vibration test for the bare pipe is shown in the following figure:

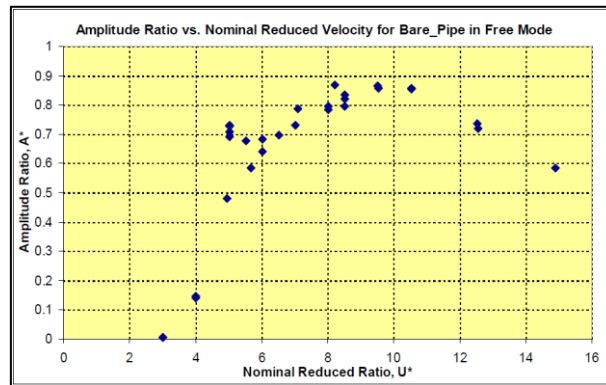


Figure 49 Amplitude of Oscillation

Using the same expression, the test results for the small-scaled model test of bare pipe and

cover is shown in the following figure:

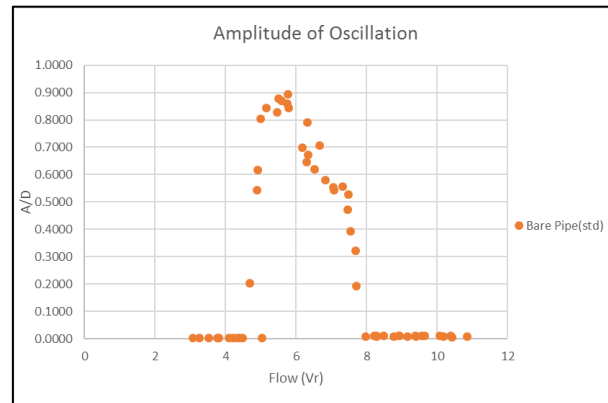


Figure 50 Amplitude of Oscillation

In the following figure, we merge the oscillation amplitude of small scaled model and the full scaled model together, it can be seen in the following figure:

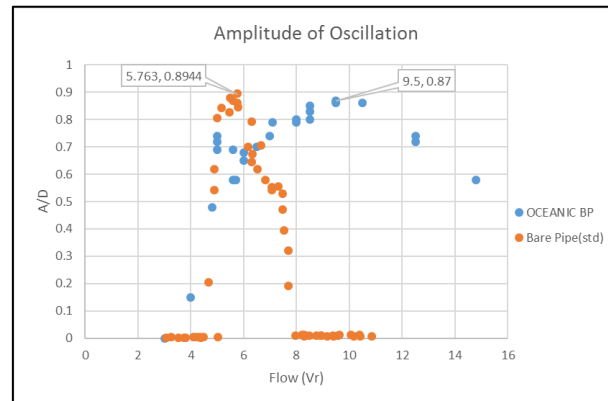


Figure 51 Amplitude of Oscillation (Merged)

In the figure of OCEANIC testing results, the oscillating amplitude will not reach 0 at the highest reduced velocity, which is due to the limitation of the test facility of the towing speed and the mass ratio of the oscillator. As it is shown in the Griffin plot, the lower the mass ratio is, the wider the synchronisation regime will be. While for the small-scaled model test, the bell shape curve is completely observed and the lock-out is shown in the figure because of the higher mass ratio of the small-scaled model test.

4.2.4. Strake Efficiency

The strake efficiency is one of the key factors which is used to evaluate the effect of the suppression in the vortex induced vibration by the strake installed on the cylinder.

In the experiment by OCEANIC, the evaluation of strake efficiency is made by calculating the percentage of oscillation reduced by the strake during the entire free vibration experiment at all the different towing speed. To calculate the strake efficiency, one needs to know the maximum amplitude of the free vibration test for the bare pipe and the strakes.

The maximum oscillation amplitude in the free vibration test for the bare pipe is $AMP = 0.87$ at $Vr = 9.6$ for the full-scaled test form OCEANIC and $AMP = 0.8944$ at $Vr = 5.763$ for the small-scaled mode test. The following figure shows the oscillation amplitude of the strake for both the small-scaled and the full-scaled model test.

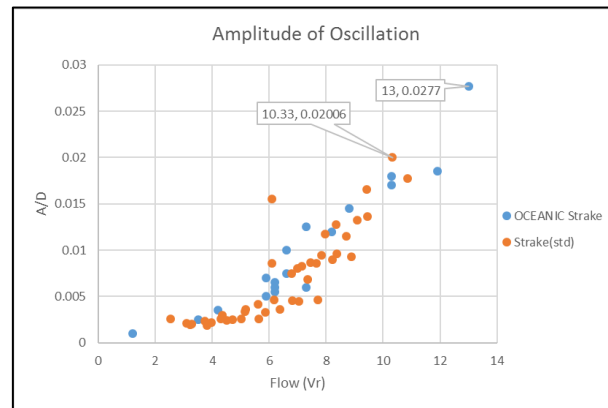


Figure 52 Oscillation Amplitude of Strake

For the small-scaled model, the maximum oscillation amplitude is $A^* = 0.02006$ at $Vr = 10.33$, while for the full-scaled strake model, the maximum oscillation amplitude lies at $Vr = 13$ and $A^* = 0.0277$. The strake efficiency η is calculated using the OCEANIC equation in the following:

$$\eta = \frac{A_{Bare(Peak)}^* - A_{Strake(Peak)}^*}{A_{Bare(Peak)}^*} \quad \text{Equation 16}$$

For the full-scaled model test from OCEANIC, the strake efficiency is:

$$\eta_{full\ scale} = \frac{0.87 - 0.0277}{0.87} = 96.816\%$$

For the small-scaled model test, the strake efficiency is:

$$\eta_{small\ scale} = \frac{0.8944 - 0.02006}{0.8944} = 97.757\%$$

The result of the strake efficiency for the small-scaled model is close to the full-scaled model, and there is a trend of decreasing for the small-scaled strake model which confirmed that the maximum oscillation amplitude of the strake model is correct. For the full-scaled model, no trend of decreasing is observed in the experiment, which indicates that the maximum oscillation amplitude could be higher than 0.0277, which will give smaller strake efficiency.

4.3. Summery

In the comparison between the small-scaled model test and the large-scaled model test, there are two parameters that should be paid more attention, which are the oscillating amplitude and the drag coefficient.

The oscillating amplitude is the key parameter for analysing the strake efficiency, by comparing the bare pipe and the strake model test results, one can get the percentage of the oscillating amplitude reduced after the installation of the strake, which is the strake efficiency. In this experiment, the small-scaled strake model shows a strake efficiency of 97.76%, while the large-scaled strake model indicates a strake efficiency of 96.82%.

The mean drag coefficient is the key parameter that can be used in the analysis of the drag force increased due to the strake. For the small-scaled model, the averaged drag coefficient before and after the installation of the strake are 1.41 and 2.23, which means an increase of 57.7%. While for the large-scaled model test, the averaged drag coefficient before and after the installation of strake model are 1.02 and 1.33 for the OCEANIC experiment, and 0.61 and 1.43 for Marin experiment, which indicates that there is an increase of 30.1% (OCEANIC) or 135% (Marin) for the drag coefficient after the installation of the strake model.

Comparing the test results of strake efficiency and the mean drag coefficient, one may find that the test results of the strake efficiency for the small-scaled model and the large-scaled model are close to each other, which indicates the significant use in the analysing of strake efficiency for small-scaled model test. While for the mean drag coefficient, the reason for the difference of the increased mean drag coefficient is mainly due to the difference in the Reynolds number in each experiment. For the small scaled model test, the Reynolds number is at a low range around 10000, while for the large-scaled model, the Reynolds number can be 10 to 100 times of the small-scaled model. The effect of the Reynolds number can be found in the literature review.

5. Wake Oscillator Model

5.1. Introduction

As the small-scaled model test only shows the oscillation under one spring stiffness and one damping ratio, it is better to use the numerical model to show how these two coefficients will influence the oscillating amplitude. For the small-scaled testing system, one possible method is using the wake oscillator model coupled with the equation of motion of one degree of freedom (1DOF).

The wake oscillator is a variable q , which satisfies the van der Pol equation. This wake oscillator is then coupled with the motion equation of the oscillator, which is a 1DOF elastically supported rigid cylinder called the structural oscillator. One can use the wake oscillator theory to define the influence of damping and spring stiffness to the oscillating amplitude.

5.2. Wake Oscillator Model

In the dimensional form, using the model from Facchinetti [18], the set of the equations are a combination of the oscillation equation of the oscillator and the equation of the wake variable. The first equation introduced here is the equation of motion for the oscillator.

$$(m + m_a) \frac{d^2 Y}{dt^2} + b \frac{dY}{dt} + kY = \frac{1}{2} \rho D V^2 L C_{VY} \quad \text{Equation 17}$$

The above equation is the 1DOF elastically rigid circular cylinder, the parameters in this equation are the mass of the oscillator m , the added mass m_a , the system damping b , the stiffness of the suspension system k , the diameter of the oscillator D , flow velocity V , the length of the oscillator L , the cross-flow force coefficient C_{VY} and the dimensional in-plan cross-flow displacement Y is then described by the linear oscillator.

The cross-flow force coefficient C_{VY} is defined by Blevins (2001)[19] as a combination of the drag coefficient C_{VD} and the drag coefficient C_{VL} :

$$C_{VY} = (C_{VD} \sin \beta + C_{VL} \cos \beta) \frac{U^2}{V^2} \text{ with } U = \sqrt{V^2 + \left(\frac{dY}{dt}\right)^2} \quad \text{Equation 18}$$

The drag and lift coefficients are the measured data from the stationary experiment, while the parameter U is the flow which is perpendicular to the cross-flow force coefficient C_{VY} . The angle β used in the equation is defined as:

Equation 19

$$\beta = -\arctan\left(\frac{dY}{dt}/V\right), \sin \beta = -\frac{dY}{dt}/U = -\frac{dY}{dt}/\sqrt{V^2 + \left(\frac{dY}{dt}\right)^2},$$

$$\cos \beta = V/U = V/\sqrt{V^2 + \left(\frac{dY}{dt}\right)^2}$$

The definition of the angle β and the decomposition of the vortex fluid force such as the drag force, lift force, along with the decomposition of the forces in horizontal and vertical direction are shown in the following figure:

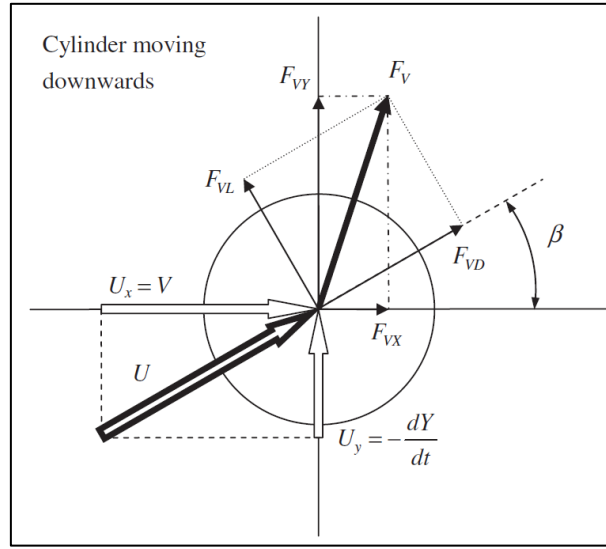


Figure 53 Definition of Angle and Forces[20]

The equation of the wake parameter is defined using the van Der Pol oscillator as:

$$\frac{d^2q}{dt^2} + \varepsilon \omega_{st}(q^2 - 1) \frac{dq}{dt} + \omega_{st}^2 q = \frac{A}{D} \frac{d^2Y}{dt^2}$$

Equation 20

Where q is the wake variable, and the ω_{st} is the Strouhal frequency which is given as $\omega_{st} = 2\pi StV/D$, where St is known as the Strouhal number. In the equation, the parameters A and ε are the tuning parameters which control the synchronisation regime and the oscillation amplitude of the wake oscillator.

Since then, we get the equation of motion for the oscillator and the equation for the wake variable. These two equations can be solved using the fourth ordered Runge–Kutta methods, which is an inbuilt function in MATLAB called “ode45”.

5.3. Free Vibration Simulation

In the wake oscillator model, after setting the tuning parameters A and ε , as well as the flow speed U , the solutions of the displacement Y and the wake variable q gave as time domain results, which can be found in Figure 54 following figure:

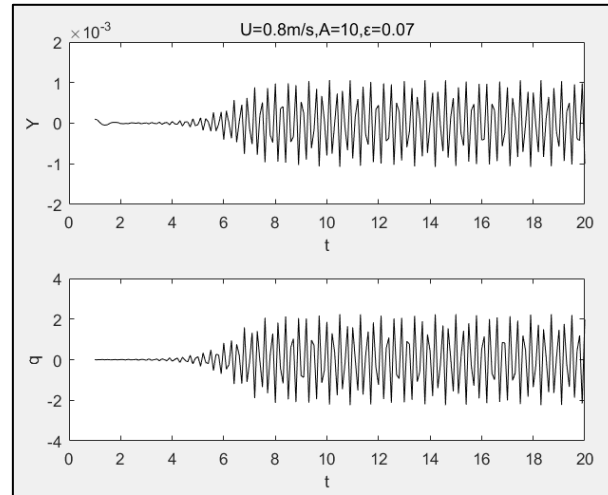


Figure 54 Wake Oscillator for 20-seconds' Simulation

In the simulation, there is one thing that should be kept in mind is that the flow speed in the simulation is kept as an increasing value, which is the same as in the experiment. To make the simulation more accuracy, the start value of parameters for the new flow velocity in the wake oscillator should be the ended value of the last flow velocity.

Then, the simulation result of the displacement Y can be used for the next procession to determine the amplitude of oscillation under the certain flow speed, which is the same method carried out in processing the results from the free vibration test. With the different follow speeds for the same tuning parameters, we get the figure of the oscillation amplitude with flow speed. Which can be used in the comparison with the free vibration test results of the small-scaled model.

In the simulation, the mass, spring stiffness and damping ratio of the wake oscillator are the same with the small-scaled model test. The parameters that vary are the tuning parameters A and ε . The idea of the simulation is to find the proper tuning parameter that can simulate the free vibration test.

For the bare pipe test, the suitable values for the tuning parameters are $A = 30$ and $\varepsilon = 0.009$, which is shown in the following figure:

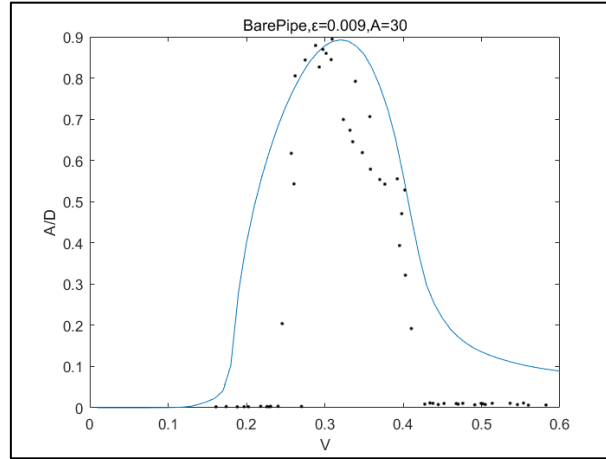


Figure 55 Wake Oscillator Simulation for Bare Pipe Test

As for the free vibration of the cover model which is shown in Figure 56, the shape of the oscillation amplitude is different from the bare pipe test. Thus, the values of the tuning parameters are also different, the most suitable combination is $A = 25$ and $\varepsilon = 0.015$.

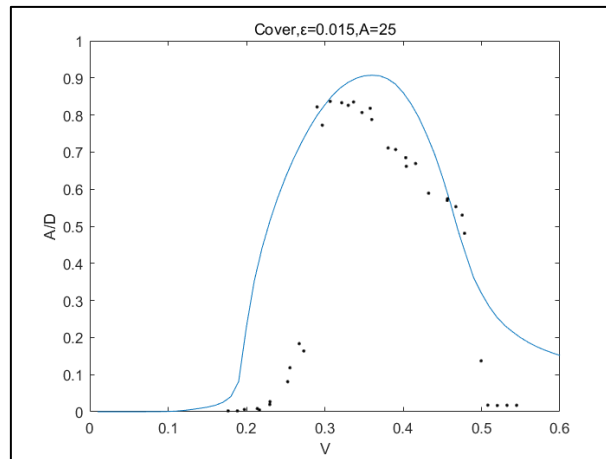


Figure 56 Wake Oscillator Simulation for Cover

It can be found that, through the two simulations, the tuning parameter changes according to the different diameters of the cylinder.

5.4. Range of Application

Before using the wake oscillator model for analysing the real model test results, the range of application shall be decided in advance, as well as the accuracy and precision.

5.4.1. Mass Ratio

In the literature study, one can know that the effect of mass ratio is mainly on the change of the lock-in range in the free vibration model test. When increasing the mass ratio, the lock-in range

will be shorter, which is known as a shorter synchronization regime, the reduced velocity of lock-out will decreasing.

Thus, for the wake oscillator, by change the set of the mass of the oscillator, the mass ratio will change along with the mass. To find out whether the wake oscillator model can simulate this phenomenon, a series of mass ratio were set and the result of the simulation is shown as the following figure:

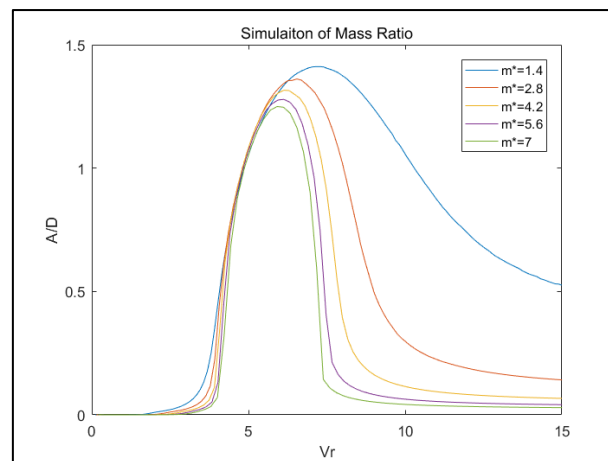


Figure 57 Effect of Mass Ratio on Wake Oscillator Model

From the above figure, one can find that with the increase of mass ratio m^* , the synchronization regime is reduced, and the reduced velocity at the lock-out is decreasing. Thus, the wake oscillator model can be used to indicate the effect of mass ratio on the lock-in range.

5.4.2. Damping Ratio

The effect of damping ratio on the on the model test, as it is known in the literature study, is to reduce the oscillating amplitude, and the peak amplitude is mostly affected by the damping ratio than other part of the oscillating amplitude.

Thus, to find out whether the wake oscillator model can indicate the change of the damping ratio, a series of damping ratio is chosen from $\zeta = 0.01$ to $\zeta = 0.04$, and the simulation results are shown in the following figure:

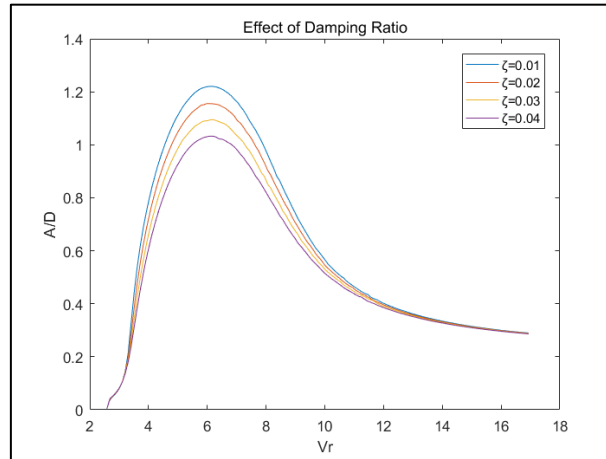


Figure 58 Effect of Damping Ration on Wake Oscillator Model

The upon figure indicates that the wake oscillator model can simulate the effect of the damping ratio on the maximum oscillation amplitude in the free vibration experiment.

5.4.3. Tuning Parameters

In the wake oscillator model, two tuning parameters A and ε are used to adjust the shape of the oscillating amplitude. These two tuning parameters have no physical meaning, thus some people may doubt whether the wake oscillator model using the tuning parameters can be used to simulate the free vibration experiment, or in other words, whether the wake oscillator model can show the similar trend of the oscillating amplitude when the parameters such as the mass ratio and the damping ratio are changed.

From the simulation on changing the mass ratio and damping ratio, it can be found that the wake oscillator model can show the correct trend of the change on the oscillating amplitude as the real model test. As the tuning parameters have no real physical meaning, then it is useful to study the relationship between the tuning parameters and the oscillating amplitude.

If we keep one of the tuning parameters as constant and change the other one, one can find that, through the two simulations, the tuning parameter changes according to the different diameter of the cylinder. If we keep one of the tuning parameters as constant and change the another one, the effect of single tuning parameter is shown in following figures:

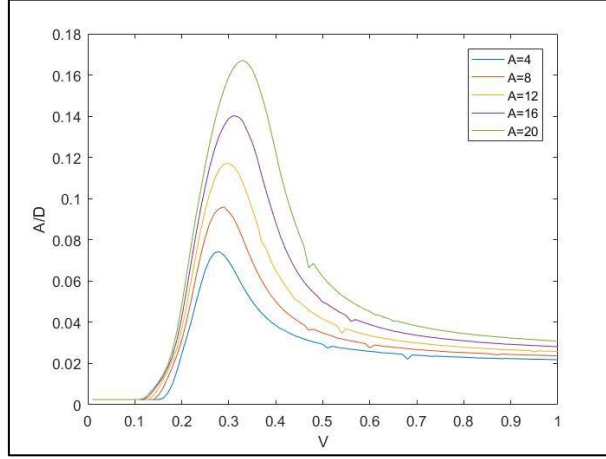


Figure 59 Effect of tuning parameter A

In the upon figure, for the effect of changing the tuning parameter A and keep all other parameters unchanged in the wake oscillator model, one can find that with the increase of A , the peak of the oscillating amplitude A/D will increase, as well as the lock-in range.

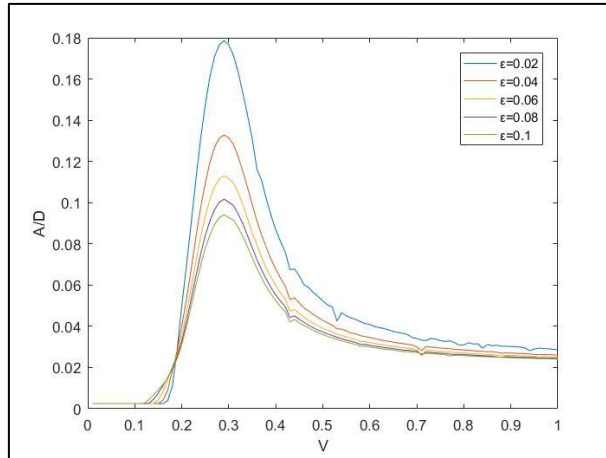


Figure 60 Effect of Tuning Parameter ε

The upon figure indicates the effect of the tuning parameter ε , it can be found that with the increase of ε , the peak of the oscillating amplitude will decrease, and the lock-in range will become wider. There is one more thing which is different from the parameter A , which is at the beginning of the figure, the amplitude will become gentle when the parameter ε increases.

However, to study the change of the tuning parameters in different experiments, it is difficult to change only one variable of the testing equipment while other variables remain unchanged. Thus, the next chapter will discuss the combination of the tuning parameters in the different experiment condition.

5.5. Tuning Parameter in Different Experiments

The current wake oscillator model does not consider the effect of Reynolds number in the

simulation, while in real model test, the Reynolds number varies in different experiment. Thus, the effect of Reynolds number on the simulation, and the influence of Reynolds number on the wake oscillator model will be introduced in the following section.

The current research of the relation of the Reynolds number in the free vibration amplitude is the research from Blevins (2009).

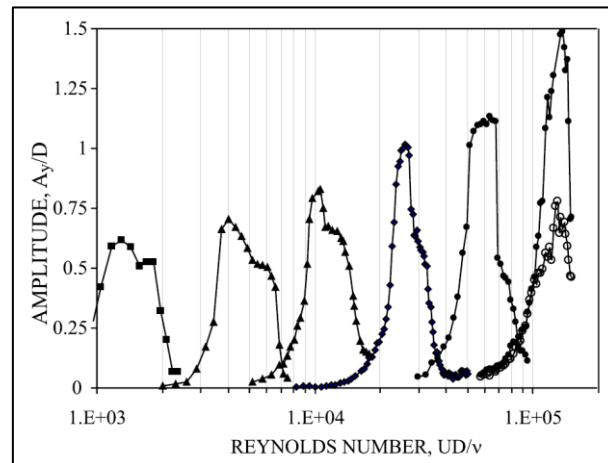


Figure 61 Experiment from Blevins (2009)

The upon figure shows the amplitude of transverse cylinder response as a function of Reynolds number. This experiment is from the research of Blevins (2009), the mass ratio of these oscillator is kept as a constant ($m/\rho D^2 = 5.02$), as well as the damping ($\zeta = 0.02m$) and the mass damping ($2m(2\pi\zeta)/\rho D^2 = 1.24$). the surface roughness of the cylinder is $k/d = 0.0001$ for the solid symbols and $k/d = 0.005$ for the open symbols. The change of Reynolds number is achieved by using cylinders with different diameters from 0.305mm to 12.7cm.

However, the x-axis cannot be switched from Reynolds number into the reduced velocity as the stiffness for each experiment is different to maintain the similar natural frequency, but the exact value of the spring stiffness is unknown from the public data.

Thus, in this part, we will use the wake oscillator model to simulate the experiment results from Lee and Bernitsas (2011)[6], who used the controlled motor instream of the spring to provide the stiffness and damping for the oscillator, which means that other parameters can maintain unchanged if one wants to change only the damping or the stiffness. The experiment results will be simulated by the wake oscillator to find out the changes of the tuning parameter in different stiffness condition.

In the experiment from Lee and Bernitsas (2011)[6], the damping of the oscillator is expressed by ζ which is the damping ratio in the water, ζ is given as:

$$\zeta = \frac{b}{2\omega_n(m + m_a)} = \frac{b}{2\sqrt{k(m + m_a)}} \quad \text{Equation 21}$$

Where b is the damping, and in the experiment of Lee and Bernitsas (2011)[6], there are two

different damping ratios which are the total damping ζ_{total} and the virtual ζ_{harn} which is generated by the motor. The expression of these two damping ratios are as following:

$$\zeta_{total} = \frac{b_{bearing} + b_{harn}}{2\sqrt{k_{vertical}(m + m_a)}}, \zeta_{harn} = \frac{b_{harn}}{2\sqrt{k_{vertical}(m + m_a)}} \quad \text{Equation 22}$$

As this experiment is designed for studying the VIVACE (VIV for Aquatic Clean Energy), and ζ_{harn} is used to describe the energy absorbed by the generator, thus, we set the $\zeta_{harn} = 0$ in the simulation, which means the $b_{harn} = 0$. Then we can calculate the system damping with the provided mass and stiffness.

The experiment of Lee and Bernitsas (2011)[6] provided a group of stiffness from $k = 400N/m$ to $k = 1800N/m$ with a step of $200N/m$, and the oscillating amplitude at $\zeta_{harn} = 0$ will be simulated using the wake oscillator, the experiment result is shown in the following figure:

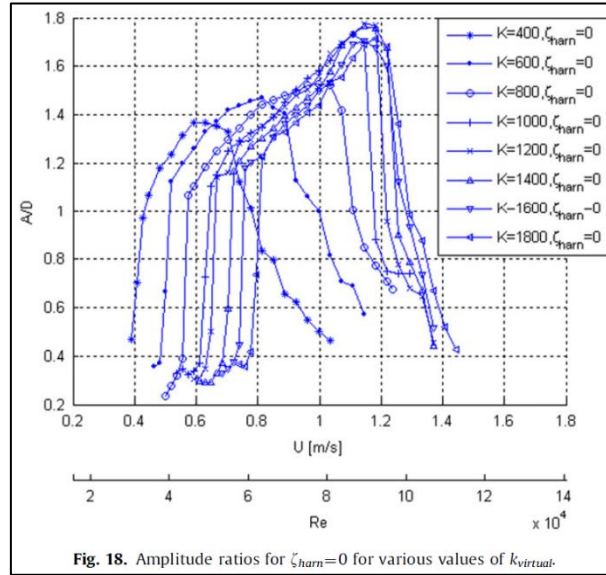


Figure 62 Experiment Results from Lee and Bernitsas (2011)[6]

For free vibration experiment, it is not a good way to explain the oscillation amplitude with the Reynolds number or the flow speed, which is due to the reason of dimensional parameters for the x-axis. Thus, a better way is to use the reduced velocity for the explanation of the oscillation amplitude, which is calculated as:

$$Vr = \frac{V}{D * f_n} = \frac{V * 2\pi}{D * \sqrt{\frac{k}{m + m_a}}} \quad \text{Equation 23}$$

The value of the parameters on the upon equation can be found in the paper, where V is the follow speed, $D = 8.89cm$ is the diameter of the cylinder, k is the value of the virtual spring stiffness varies from $400N/m$ to $1800N/m$, $m = 8.88kg$ and $m_a = 5.67kg$ are the mass and added mass of the oscillator respectively. Then the oscillating amplitude can be switched from velocity to the non-dimensional form as reduced velocity.

In the expression of the paper, it can also be found that the as the damping coefficient of the

bearing is regarded as a constant $c_{bearing} = 4.4$, and the damping ratio changes according to the different virtual spring stiffness, which is calculated as:

$$\zeta = \frac{c_{bearing}}{2\sqrt{(m + m_a) * k_{virtual}}} \quad \text{Equation 24}$$

The upon equation indicates that, with the system damping coefficient as a constant, the damping ratio reduces with the increase of the spring stiffness. Thus, the plot of oscillating amplitude in reduced velocity with eh damping ratio is shown in the following:

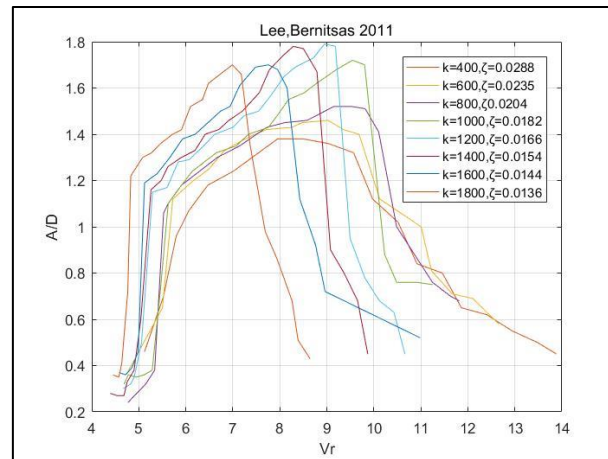


Figure 63 Experiment of Lee, Bernitsas(2011), Switch the Reynolds Number Into Reduced Velocity

When switching from the velocity or the Reynolds number to the reduced velocity, it can be found that the oscillating amplitude is different when expressed in a non-dimensional form. Then we use the wake oscillator to simulate this experiment by setting the parameters under the same value.

The range of Reynolds number for each experiment is shown as the following table:

Table 15 Range of Reynolds Number on Each Test

K(N/m)	ζ	Re(Start)	Re(End)
400	0.0288	3.0E+04	8.0E+04
600	0.0235	3.5E+04	9.0E+04
800	0.0204	4.0E+04	1.0E+05
1000	0.0182	4.2E+04	1.1E+05
1200	0.0166	4.5E+04	1.1E+05
1400	0.0154	4.6E+04	1.1E+05
1600	0.0144	5.5E+04	1.1E+05
1800	0.0136	6.0E+04	1.2E+05

The free vibration model test indicates that, at a higher range of Reynolds number, the shape of the oscillating amplitude is changed as the lock-in range is reduced, the lock-out happens at a lower reduced velocity, and the peak value of the oscillating amplitude is increase then decreased. In the upon figure, one may notice that the damping ratio of each experiment is

different, which is lower at the higher Reynolds number, this fact will not influence the evaluation of the effect of the Reynolds number on the oscillating amplitude in free vibration experiment. The change of the synchronization regime in the upon experiment is mainly due to the increase of the Reynolds number, as it is known that when the damping ratio is reduced, the lock-in range should be increased as well as the reduced velocity when lock-out happens.

The simulating results, for the wake oscillator, does not completely satisfy the experiment results. When the spring stiffness and the Reynolds number is at a lower range ($Re \in [3 \times 10^4, 8 \times 10^4]$), the wake oscillator model is capable to simulate the experiment results, which is shown as following figure:

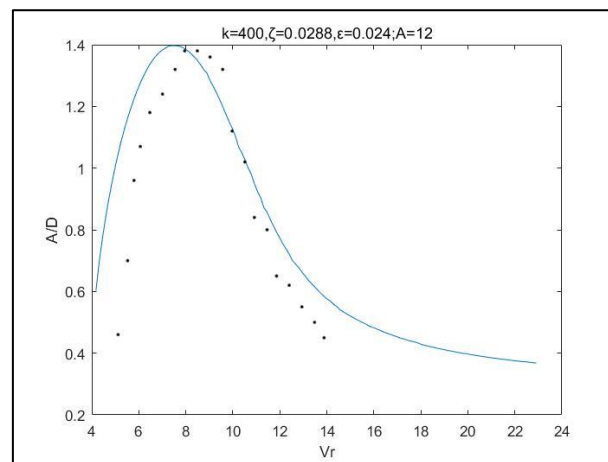


Figure 64 Wake Oscillator Simulation under Reduced Velocity

If we use the same tuning parameter ($A = 12, \varepsilon = 0.024$) of the upon simulation and change the spring stiffness, the oscillating amplitude will be as:

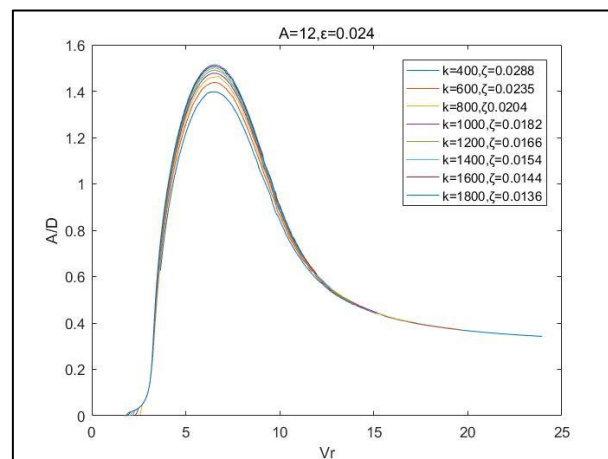


Figure 65 Wake Oscillator Simulation under Constant Tuning Parameters

The upon figure indicates that if the tuning parameters are kept constant, then the simulation results are quite different from the actual experiments. This indicates that for one combination of tuning parameters, the change of spring stiffness and damping ratio cannot be simulated

when we keep the tuning parameters unchanged.

The simulation of the wake oscillator is then using different combination of tuning parameters ε and A , to get the same lock-in range and peak amplitude. The combination of tuning parameters on different tests can be found in the appendix. The following table is the value of the chosen tuning parameters:

Table 16 Combination of Tuning Parameters

K(N/m)	ζ	Re(Start)	Re(End)	ε	A
400	0.0288	3.0E+04	8.0E+04	0.024	12
600	0.0235	3.5E+04	9.0E+04	0.028	13.5
800	0.0204	4.0E+04	1.0E+05	0.022	12
1000	0.0182	4.2E+04	1.1E+05	0.01	8
1200	0.0166	4.5E+04	1.1E+05	0.007	6
1400	0.0154	4.6E+04	1.1E+05	0.006	5.5
1600	0.0144	5.5E+04	1.1E+05	0.005	4.4
1800	0.0136	6.0E+04	1.2E+05	0.004	3.5

The upon table shows the trend of the change on the tuning parameters with the increase of the Reynolds number and the decrease of the damping ratio.

While for the free vibration experiment under higher Reynolds number range ($Re \in [8 \times 10^4, 1.4 \times 10^5]$), the shape of the oscillating amplitude is different from the smaller spring stiffness one. From the switched figure, we can find that for the low Reynolds number tests, the oscillating amplitude is a bell-shape curve, while for the higher range of Reynolds number, the oscillating amplitude is not a symmetric bell-shape curve, there will be a drop of the oscillating amplitude when reaching the peak amplitude, and this phenomenon cannot be simulated by the wake oscillator model. One example is shown as:

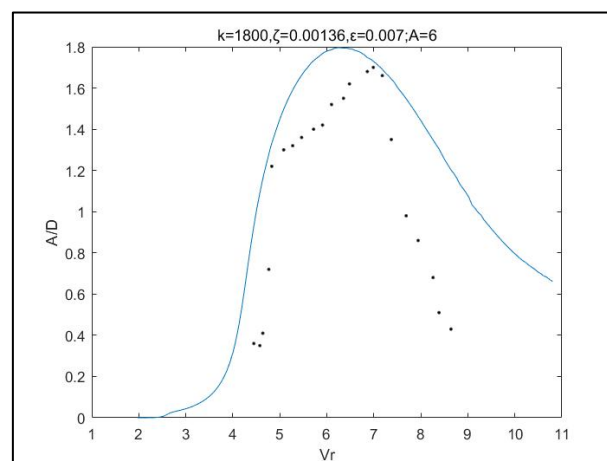


Figure 66 Wake Oscillator Simulation for $k=1800\text{N/m}$ under Reduced Velocity

The upon figure shows the amplitude of transverse cylinder response as a function of Reynolds number. This experiment is from the research of Blevins (2009), the mass ratio of these oscillator is kept as a constant ($m/\rho D^2 = 5.02$), as well as the damping ($\zeta = 0.02m$) and the

mass damping ($2m(2\pi\zeta)/\rho D^2 = 1.24$). the surface roughness of the cylinder is $k/d = 0.0001$ for the solid symbols and $k/d = 0.005$ for the open symbols. The change of Reynolds number is achieved by using cylinders with different diameters from 0.305mm to 12.7cm.

However, the x-axis cannot be switched from Reynolds number into the reduced velocity as the stiffness for each experiment is different in order to maintain the similar natural frequency, but the exact value of the spring stiffness is unknown according to the public data from the public data. Thus, two parameters are changed in this experiment, the diameter and the spring stiffness.

5.6. Summary

For the free vibration experiment, the current research for the effect of Reynolds number is focusing on the peak amplitudes, which is also known as the “Griffin Plot”. But the shape of the oscillation amplitude and the lock-in range of the reduced velocity under different Reynolds number has not been considered.

In the simulation of the wake oscillator model, it can be found that the combination of the tuning parameters cannot satisfy all the experiment when the value of spring stiffness and the damper are set in the same value as the experiments. The oscillating amplitude, under higher Reynolds number (this is achieved by using higher spring stiffness and reduce the damping ratio, but the mass ratio is kept unchanged), is not shown as the bell-shape curve, which cannot be simulated by the wake oscillator. This indicates that the effect of Reynolds number should not be ignored in the free vibration experiment.

The advantage of using the wake oscillator model to simulate the free vibration model test is that the wake oscillator model can simulate the oscillation in the time domain, rather than frequency domain, which does not require the pre-set of the oscillating frequency of the oscillator.

From the simulation results, it can be found that, the wake oscillator model indicates the same trend of the oscillating amplitude when the characters such as the mass ratio or the damping ratio is changed. For the effect of Reynolds number, the wake oscillator model indicates the trend of the tuning parameters as the tuning parameters will both decrease at a higher Reynolds number range. Although the damping ratio is also changing in the experiment, the decrease of the lock-in range is mainly from the effect of Reynolds number, and using the proper combination of tuning parameters, this effect can be shown.

6. Testing Facilities Design

In this chapter, suggestions will be given for the flume design and the operating of the small-scaled model test.

6.1. Comparison of the Flume and Towing Tank

6.1.1. Fluid Velocity

Tow speed

One of the most obvious benefit of towing tank is the accuracy in the control of towing speed, as the fluid in the towing tank is still while the model is moving through the carriage which is overhead of the tank. Thus, for a towing tank, the flow speed of the model is exactly the towing speed of the carriage. For the high-speed towing tank from MARIN, the towing speed can reach 15m/s of maximum tow speed and a maximum tow force of 10 kN under the tow speed of 4m/s due to the power limit of the engine installed in the carriage.

Flume flow

The flow velocity of the flume depends on the capability of the water pump and the section area of the flume. Taking the example of the flume in TU Delft, the maximum flow speed for the long flume ($14.3\text{m} \times 0.4\text{m} \times 0.4\text{m}$) is 0.65m/s at the discharge rate of 85L/s . While measuring the flow rate of the flume, due to the restriction of the flume size, the flow rate is not even at everywhere for the same section area. This is due to the viscosity of the water which forms a boundary layer in the flume. This layer has a limited influence on the flow rate of the flume as is estimated with a scale of 10^{-3} meter thickness when the Reynolds number is reaching $Re = 10^4$ [16].

The other problem while measuring the flow rate of the flume is that although one may calculate the flow speed of the water in the flume by knowing the discharge rate of the pump and the section area of the flume, the exact flow speed may be different from the calculated results due to the unstable reading in discharge rate, which usually happens during the flume experiment and the discharge rate is used only when naming the recorded data.

Thus, to get the exact speed of the water flow in around the testing model, one proper way is to install a flow meter in the middle of the section area of the flume with the same water depth of the mode, the place is recommended to be around 1m upstream of the model in a 10m long flume. If the flume is not long enough in the experiment, the distance between the model and the flow meter can be reduced but it should be tested with a reagent to ensure that the distance is enough to avoid the disturbing of water flow by the flow meter. For the material of the reagent, potassium permanganate (KMnO_4) is recommended as it is efficiency and commonly used in the experiment.

6.1.2. Testing Time

Waiting time of towing tank

For the towing tank, as recommended by MARIN, a minimum waiting time of 5 minutes is

required after each test to absorb the energy transferred to the water through the last experiment. According to the previous study of waiting time by MARIN, a longer waiting time will not make any significant contribution to the experiment, thus considering the efficiency of the experiment, 5 minutes' waiting time is needed for each experiment.

Time of towing test

The total length of the towing tank from MARIN is 210m, and the effective length for the experiment is 180m. The highest towing speed during the experiment is $2.5m/s$ while the lowest is $0.3m/s$, from which one may know the towing time can be 72s for the highest towing speed and 10 minutes under the lowest towing speed condition. Added with the waiting time between each test, the total testing time for one experiment in the towing tank could be 6 to 15 minutes.

Waiting time for flume

The test of flume is different from the towing tank as one can change the flow speed directly after the measurement of the previous flow speed by increasing or decreasing the discharge rate of the flume.

In the testing procedure of flume, the waiting time is only needed when the testing type or the testing model need to be changed. The length of the waiting time depends on the installation of the testing facilities and calibration. In the testing, for one speed, the time for measurement is 2 minutes, and the waiting time for the water flow to become steady after increase the discharge rate is 1 to 2 minutes. Thus, for one testing speed, the test duration is 3 to 4 minutes.

6.1.3. Testing Ability

Measuring accuracy

The towing tanks used for the full-scaled model test are normally member organisations of International Towing Tank Conference (ITTC), and the testing accuracy of the towing carriage is thus guaranteed. Besides, for the large-scaled model, it is much easier to control the surface roughness and the parameters of the testing facility such as the spring stiffness and the mass ratio.

For the small-scaled model test in the flume, the main problem during the experiment that influence the measuring accuracy is the noise signal from the load cell. The source of the noise can be divided into two parts, the first part is the amplifier, which requires a more stable power source. The other one is from the load cell because of the inner force generated by the deformation of the testing frame.

Reynolds number

The most obvious difference in the towing test and the flume is on the Reynolds number, as the Reynolds number is related with the diameter of the cylinder, for the full-scaled model test, the Reynolds number can reach as high as $Re = 8 \times 10^5$, which is closer to the real condition of a riser in the ocean. For the other towing tank test from OCEANIC, the range of Reynold number is $10^5 < Re < 1.2 \times 10^6$ when testing the drag coefficient of the model, which makes it able to achieve the critical Reynolds number regime.

Due to the limited diameter of the small-scaled model and the limited flow speed, the Reynolds number that the flume can reach is lower than the towing tank. In the previous experiment, the maximum Reynolds number one can reach is $Re = 1.6 \times 10^4$, and the range of Reynolds number the flume can achieve is $6000 < Re < 1.6 \times 10^4$, which is within the subcritical Reynolds number regime.



The following table is a summary for the upon comparison of the testing ability and time of the towing tank and the flume, from which one can have a better understanding of the difference between the testing facilities.

6.1.4. Results Evaluation for Strakes

The strake design is evaluated by comparing the testing results of the bare pipe and the strakes. As introduced in the dissertation, the VIV strake efficiency is defined as the reduction of the oscillation amplitude due to the strakes in the free vibration test.

Except for the strake efficiency, another important parameter for the strake is the drag coefficient. As it is known to all, the advantage of the strakes is the high efficiency of the VIV suppression, while the main disadvantage of the strake is the increase of the drag coefficient, which can be measured in the stationary test. The following table is the comparison of the low and high scale model of the bare pipe and the strake model.

Table 17 The Comparison of the Large and Small Scaled Model Test

	Large scale model	Small scale model
Type of experiment	Stationary, Free vibration	Stationary, Free vibration
Place of experiment	OCEANIC, MARIN	TU Delft
Testing facility	Towing tank	Flume
Testing model		
Reynolds number	$10^5 \sim 1.2 \times 10^6$ (OCEANIC) $1.5 \times 10^5 \sim 8 \times 10^5$ (MARIN)	$6000 \sim 2 \times 10^4$
Testing speed	2.5m/s Max	0.55m/s Max
Test duration	6 to 15 minutes per speed	3 to 4 minutes per speed
Oscillation amplitude (A/D)	0.87 for bare pipe 0.0277 for strakes	0.9844 for bare pipe 0.02006 for strakes
Strake efficiency	96.816%	97.757%

Drag coefficient (Averaged)	1.02 for bare pipe (OCEANIC) 1.33 for strakes (OCEANIC) 0.61 for bare pipe (MARIN) 1.43 for strakes (MARIN)	1.41 for bare pipe 2.24 for strakes
Increased drag (% of bare pipe)	30.4% (OCEANIC) 134.4% (MARIN)	58.9%

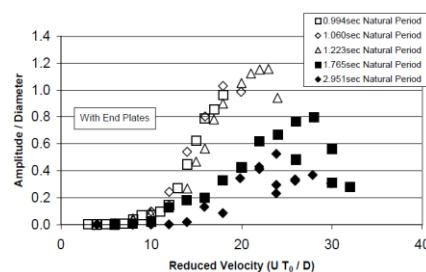
6.1.5. VIV Fairings

In the experiments of this dissertation, there is no experiment for the fairings, thus, the study from Slocum (2004)[17] on the flutter instability in riser fairings. In this study, both high scale model and low scale model were tested. The following table is the introduction and comparison of the high and low scale fairing model test:

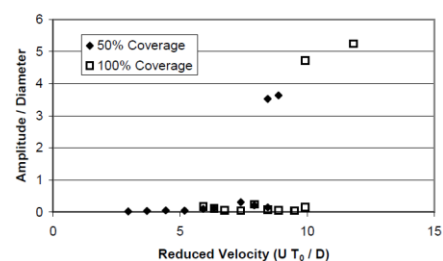
Table 18 Large and Small Scaled Fairing Model Test

	High scale model test	Low scale model test
Location	David Taylor Model Basin (DTMB)	MARINTEK
Testing facility	Towing tank	Rotating test rig
Types of tests	Free vibration	Free vibration, Rigid cylinder test
Size of cylinder	D=220mm, L=3.96m	D=20mm, L=9.63m,
Fairing size	Span=61.2cm, Chord length=52.6cm, Nose diameter=23.2 cm	Span=87.4mm, Chord length=82.8mm, Nose diameter=36mm
Reynolds number	$Re=1 \times 10^6$	$Re=4 \times 10^4$
Flow type	Constant towing speed	Linear shear flow, upper end is 14% higher of the flow speed than the lower end
Flow speed	4.5m/s	1.2m/s

Testing result

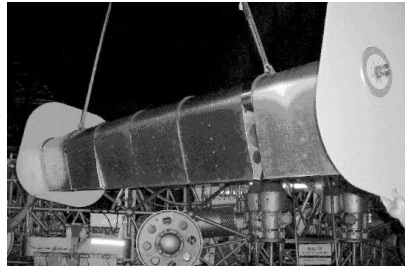


DTMB tests results of rigid spring-mounted cylinder with fairings



long flexible cylinder with fairings in the linearly sheared flow

Testing
model



6 fairings with end plate



Fairings for long flexible cylinder

It can be found that, for the high scale model test, only the free vibration test is conducted and the towing tank can achieve both high Reynolds number and high reduced velocity. While for the low scale model, two types of tests are conducted, one is the free vibration test which is the same with the high scale model test, the other is the rigid cylinder test.

In this research, due to the need of studying the flutter instability, the low scale model is used for studying the modes of vibration for the long flexible cylinder due to the fairings, as the high modes will reduce the fatigue life of the cylinder due to the higher shear stress. The low scale model is with a length of 9.63m, which is long enough for the observation of the first mode vibration, and cannot be found in the high scale model test in this study.

6.2. Flow Rate

The flow rate is one of the key design requirements of the flume, as it has a wide relation with the model and size of the flume. To evaluate the maximum flow speed that the flume can achieve, one needs to take the following parameters into consideration.

6.2.1. Critical Mass Ratio

Mass ratio is highly related to the oscillating synchronisation regime of the free vibration test, if one wants to observe the complete bell-shape curve of the oscillation amplitude with the reduced velocity, the flow rate of the flume must be high enough to meet the demand of the reduced velocity to achieve the lock-out range.

Through the research by Govardhan & Williamson (2004)[1], the relationship for the mass ratio and the range of the synchronisation is shown in the following figure:

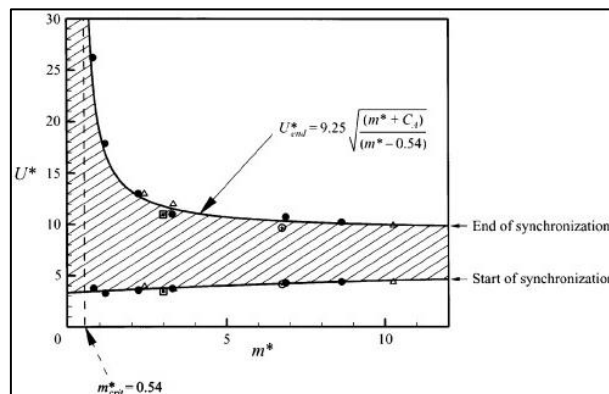


Figure 67 Synchronisation Regime with Mass Ratio

In the figure, the start of the synchronisation is at $U^* = 3 \sim 5$, while the U_{end}^* marks the upper boundary of the shaded synchronisation regime, and it can be calculated by the following equation:

$$U_{end\ of\ synchronization}^* = 9.25 \sqrt{\frac{m^* + 1}{m^* - 0.54}} \quad \text{Equation 25}$$

Thus, if one can get the mass ratio of the oscillator, the required reduced velocity for lock-out can be calculated, and thus one knows the required highest flow speed of the flume.

6.2.2. Reduced Velocity

In the equation of calculating the lock-out flow rate, it should be noticed that if the mass ratio of the oscillator is smaller than the critical mass ratio, the synchronisation will continue when the reduced velocity increases and there will be no lock-out for the oscillator. The critical mass ratio is given as: $m_{CRIT}^* = 0.54 \pm 0.02$.

Here, the U^* used in the equation has the same expression of the Vr used in the experiment, both are the expression of the reduced velocity, and Vr is calculated as:

$$Vr = \frac{V}{NatFreqWet * D} \quad \text{Equation 26}$$

Where V is the mean value of the flow meter placed in the same water depth of the model, the $NatFreqWet$ is the natural frequency calculated in the free vibration for the cylinder in the water and D is the diameter of the oscillator. Thus, the mean flow rate under the reduced velocity is:

$$V = Vr * NatFreqWet * D \quad \text{Equation 27}$$

Thus, to decide the flow rate of the flume by the given mass ratio and natural frequency of the oscillator, the procedure is shown in the following figure:

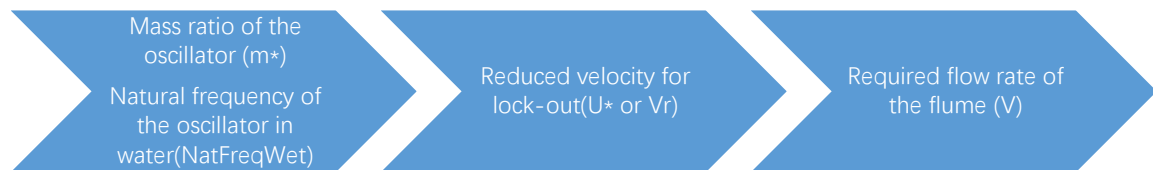


Figure 68 Calculating procedure

Since one knows the flow rate of the flume, the pumping power can be calculated, which gives the basis of designing the proper pumping system.

6.2.3. Measuring of Flow Rate

The measuring method for the small-scaled model test in the flume is different from the large-scaled model test in the towing tank. For the towing tank, the fluid remains static while the

model is towed by the carriage above the tank and driven by electric engine, thus the towing speed equals to the water flow speed. For example, the towing tank in MARIN is 210m long, and the maximum towing speed for the carriage is $15m/s$ as introduced.

While for the small-scaled testing facility, the flow rate is restricted due to the pumping power and the boundary layer due to the water flow in the flume. Thus, to ensure the accuracy of the flow rate, the flow meter shall be placed in the middle of the two walls of the flume, and in the same water depth where the model is placed. In the experiment, the maximum flow rate the flume can achieved is $0.6m/s$ as the flow meter measured.

6.3. Flume Size

6.3.1. Length of Flume

The length of the flume should meet the demand for both the installation of the testing facilities and the accuracy of the measuring.

In the experiment, to get the accurate flow rate, the flow meter is placed upstream of the oscillator, which is one fourth of the total length of the flume, and the oscillator is placed in the middle of the flume. The potential sources of disturbing the water flow could from the flow meter and the head of the water channel. Thus, the flume should provide enough gap length for the water flow to become steady before reaching the flow meter, and ensure there is no disrobing of water flow before reaching the oscillator. One testing method to define whether the gap distance meets the demand is placing the flow meter in the flume, and let the coloured water flow through the flow meter and whether the wake still exits when reaching the oscillator. An empirical data is that 1m in the flume should be enough for the gap to avoid the influence.

As for reference, the length of the flume in the experiment is 14.5m. But it is not a wise choice to make the flume too long, which may take more time to fill the flume for calibration and measuring the natural frequency of the oscillator in the water.

6.3.2. Width of Flume

The width of the flume should meet the demand of the aspect ratio of the model, and the boundary layer of the water flowing along the side wall.

The width of the flume shall make enough space for the installation of the inner frame of the oscillator, and meets the demands if one wants a model with higher aspect ratio. From the opinion of the boundary layer theory, the water flow along the flume wall is not constant but increase from 0 to the flow speed. Thus, increasing the gap for the inner frame and the wall of flume is a significant method to reduce the difference of flow speed.

A wider flume will require higher pumping power, and stronger structural design. The example of the flume width of the water lab is two types, one is $40cm \times 40cm$ and the other is $100cm \times 100cm$ of the section area.

6.4. Suggestions

6.4.1. Resistance

In the original testing facility, the connection between the inner and outer frame is achieved by using the frictionless table, but in real test, the friction force for the frictionless table is still high enough to influence the free vibration test, which makes the oscillation start at a higher flow speed than expected.

The suggestion for reducing the resistance during the free vibration test is replacing the frictionless table by air bearings, which can be found in the following figure:

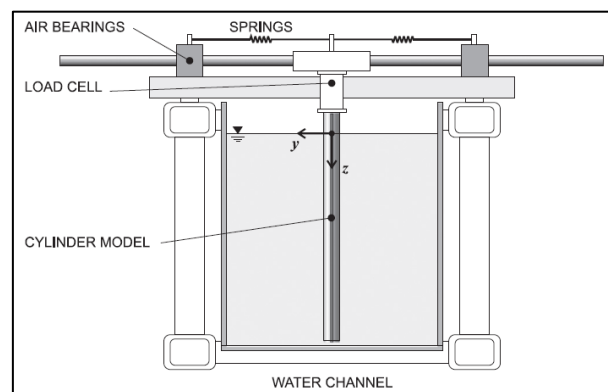


Figure 69 Air Bearings for Free Vibration Test Facility[21]

For each side of the frame, two or four air bearings should be enough to provide enough support for the inner frame to oscillate under the transverse flow.

6.4.2. 2D Test

The current testing facility is not capable for doing free vibration test under two degrees of freedom as the original frame is suitable for only one degree of freedom. For two degrees of freedom, the testing model is recommended to be hanged vertically to reduce the effect of gravity. And the possible design of the testing facility would be like the following figure:

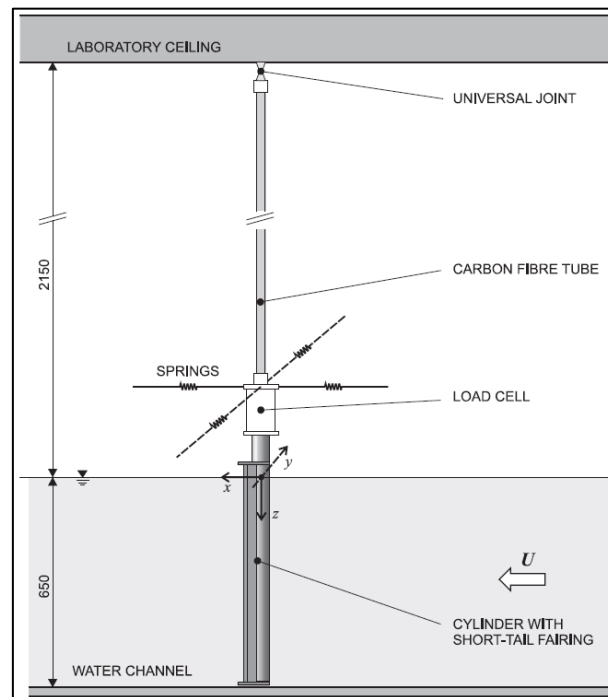


Figure 70 Two Degrees of Freedom Testing Facility

Thus, for the two degrees of freedom testing facility, the cylinder model is hanged vertically providing enough space for the connection with the testing model to the tube and the universal joint. The motion of the cylinder on transverse and along the water flow can be measured with optic laser, the drag and lift force can also be measured using the load cell.

The length of the testing model is decided according to the depth of the flume, and the oscillating amplitude should not exceed half of the width of the flume. The crushing of the cylinder model to the flume wall can be avoided by adjusting the diameter of the model.

6.4.3. Fairing Model

The research on fairing model is different from the strake model, as in the VIV fairing, the flutter instability will be observed when the fairings meet the shear flow. One disadvantage of the flume is that the flume cannot provide shear flow for the testing model, and the suggestion for the study of flutter instability is to use the rotation rig which is shown as the following figure:

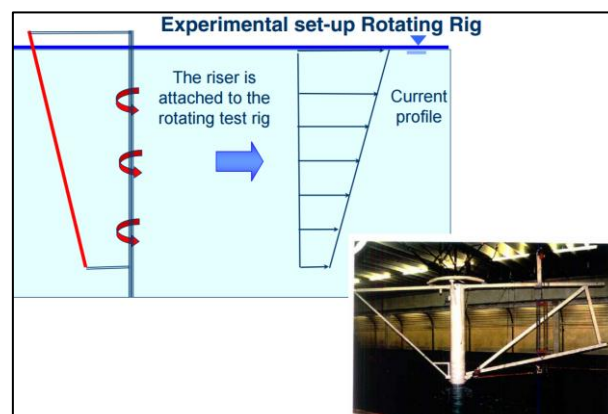


Figure 71 Rotation Rig for Fairing Model[23]

The upon figure is from the MARINTEK, which is used to study the flutter instability. The slope angle can be adjusted to provide different shear flow speed.

7. Conclusion and Recommendation

7.1. Conclusion

The small scaled model testing facility is suitable for evaluating the strake efficiency under small scaled model. The drag coefficient measured by this testing facility is higher than the large scaled model test carried out by the towing tank, the reason for causing the difference is due to the different range of Reynolds number.

Wake oscillator model is also used in this thesis to find out the parameter that will influence the tuning parameter A and ε of the wake oscillator. In the simulation of free vibration test by the wake oscillator, the combinations of tuning parameters under different range of Reynolds number are given to indicate the relationship between the tuning parameters and the Reynolds number.

7.2. Recommendation

For the small scaled model testing facility, the current testing facility in the flume or water channer can provide a limited performance on the small scaled model test such as the one degree of freedom free vibration test, and the stationary test. For the two degrees of freedom free vibration test, the testing facility is recommended as a vertical model with universal joint.

For the studying of the flutter instability, which the shear flow cannot be simulated by the flume, the rotating rig is the proper facility.

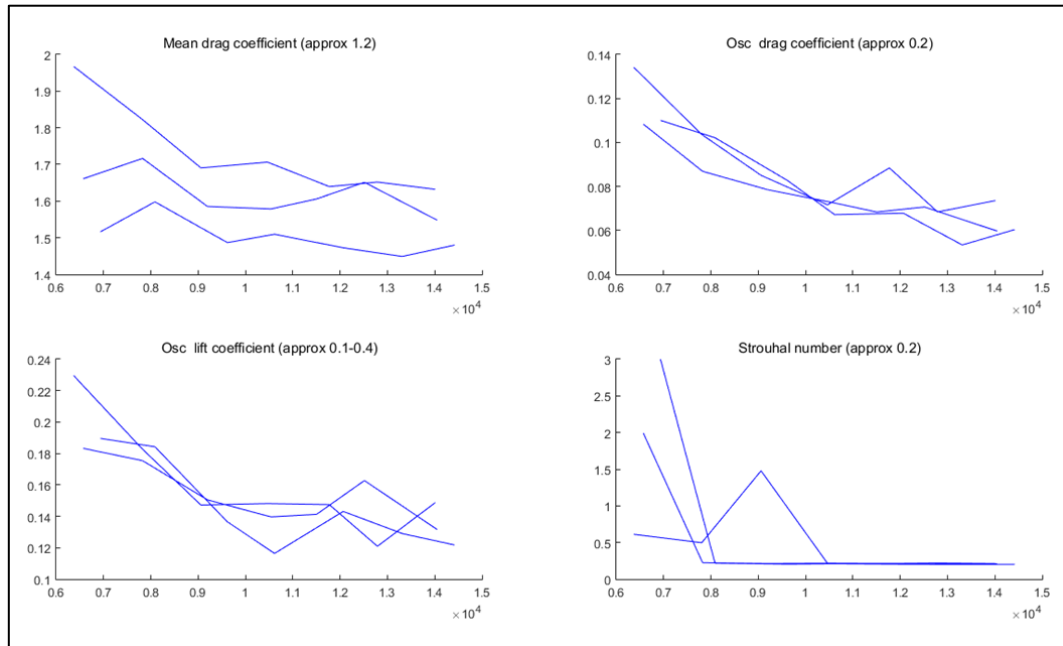
Reference

- [1] Williamson, C. H. K., and R. Govardhan. "Vortex-induced vibrations." *Annu. Rev. Fluid Mech.* 36 (2004): 413-455.
- [2] Blevins, Robert D., and Charles S. Coughran. "Experimental investigation of vortex-induced vibration in one and two dimensions with variable mass, damping, and Reynolds number." *Journal of Fluids Engineering* 131.10 (2009): 101202.
- [3] Khalak, A., and C. H. K. Williamson. "Motions, forces and mode transitions in vortex-induced vibrations at low mass-damping." *Journal of fluids and Structures* 13.7 (1999): 813-851.
- [4] Lee, J. H., and M. M. Bernitsas. "High-damping, high-Reynolds VIV tests for energy harnessing using the VIVACE converter." *Ocean Engineering* 38.16 (2011): 1697-1712.
- [5] Raghavan, K., and M. M. Bernitsas. "Experimental investigation of Reynolds number effect on vortex induced vibration of rigid circular cylinder on elastic supports." *Ocean Engineering* 38.5 (2011): 719-731.
- [6] Lee, J. H., and M. M. Bernitsas. "High-damping, high-Reynolds VIV tests for energy harnessing using the VIVACE converter." *Ocean Engineering* 38.16 (2011): 1697-1712.
- [7] Pastò, S. "Vortex-induced vibrations of a circular cylinder in laminar and turbulent flows." *Journal of Fluids and structures* 24.7 (2008): 977-993.
- [8] Govardhan, R. N., and C. H. K. Williamson. "Defining the 'modified Griffin plot' in vortex-induced vibration: revealing the effect of Reynolds number using controlled damping." *Journal of Fluid Mechanics* 561 (2006): 147-180.
- [9] Achenbach, E., and E. Heinecke. "On vortex shedding from smooth and rough cylinders in the range of Reynolds numbers 6×10^3 to 5×10^6 ." *Journal of fluid mechanics* 109 (1981): 239-251.
- [10] Vandiver, J. Kim, V. Jaiswal, and V. Jhingran. "Insights on vortex-induced, traveling waves on long risers." *Journal of Fluids and Structures* 25.4 (2009): 641-653.
- [11] Ding, Z. J., et al. "Lift and damping characteristics of bare and straked cylinders at riser scale Reynolds numbers." *Offshore Technology Conference*. Offshore Technology Conference, 2004.
- [12] Roshko, Anatol. "Experiments on the flow past a circular cylinder at very high Reynolds number." *Journal of Fluid Mechanics* 10.03 (1961): 345-356.
- [13] Allen, H. Julian, and Walter G. Vincenti. "Wall interference in a two-dimensional-flow wind tunnel, with consideration of the effect of compressibility." (1944).
- [14] Fage, Arthur, and J. H. Warsap. *The effects of turbulence and surface roughness on the drag of a circular cylinder*. HM Stationery Office, 1930.
- [15] Facchinetti, Matteo Luca, Emmanuel De Langre, and Francis Biolley. "Coupling of structure and wake oscillators in vortex-induced vibrations." *Journal of Fluids and structures* 19.2 (2004): 123-140.
- [16] 董曾南 孙厚钧 宋传琳 陶晓峰. "明流光滑平板边界层特性." *力学学报* 18.6 (1982): 528-537.
- [17] Slocum, S. T., et al. "Flutter instability in riser fairings." *Offshore Technology Conference*. Offshore Technology Conference, 2004.

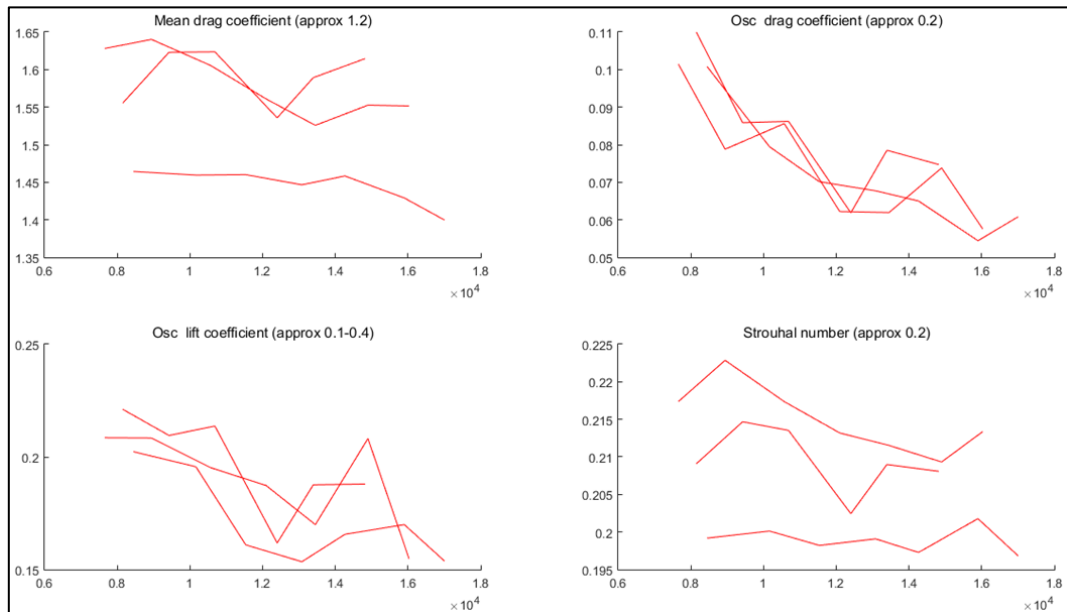
- [18] Facchinetti, Matteo Luca, Emmanuel De Langre, and Francis Biolley. "Coupling of structure and wake oscillators in vortex-induced vibrations." *Journal of Fluids and structures* 19.2 (2004): 123-140.
- [19] R.D.Blevins, in: *Flow-Induced Vibration*, second ed, Krieger Publishing Company, Malabar, 2001.
- [20] Ogink, R. H. M., and A. V. Metrikine. "A wake oscillator with frequency dependent coupling for the modeling of vortex-induced vibration." *Journal of Sound and Vibration* 329.26 (2010): 5452-5473.
- [21] Assi, Gustavo RS, and Peter W. Bearman. "Transverse galloping of circular cylinders fitted with solid and slotted splitter plates." *Journal of Fluids and Structures* 54 (2015): 263-280.
- [22] Assi, Gustavo RS, Peter W. Bearman, and Michael A. Tognarelli. "On the stability of a free-to-rotate short-tail fairing and a splitter plate as suppressors of vortex-induced vibration." *Ocean Engineering* 92 (2014): 234-244.
- [23] http://www.sintef.no/globalassets/project/marintek-seminar/presentations/viv-highlights_baarholm_rev01.pdf

Appendix A

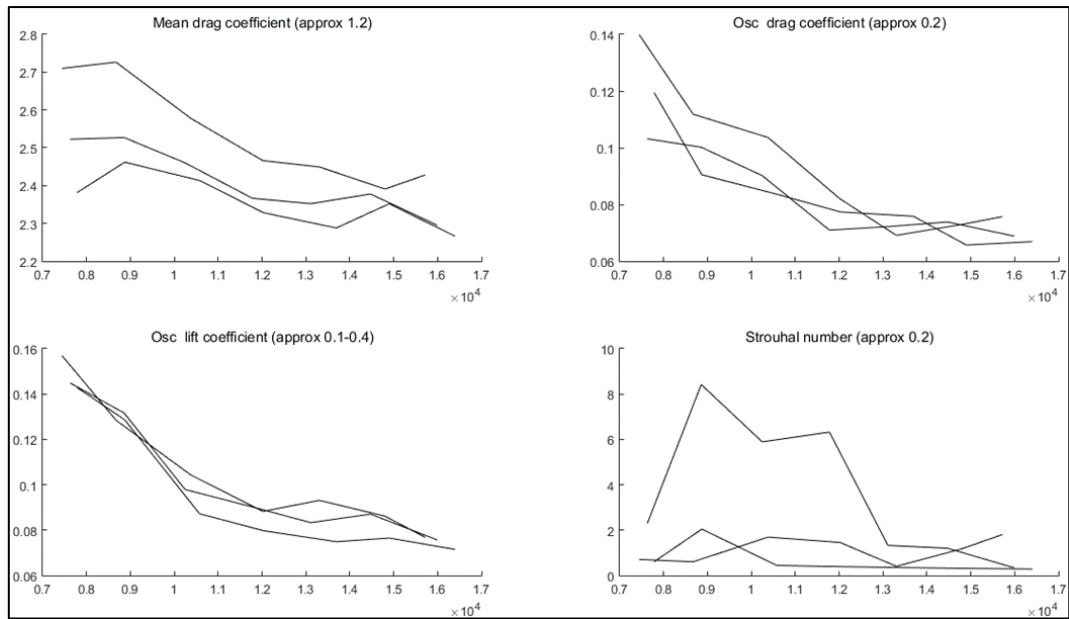
Figures for Test Results



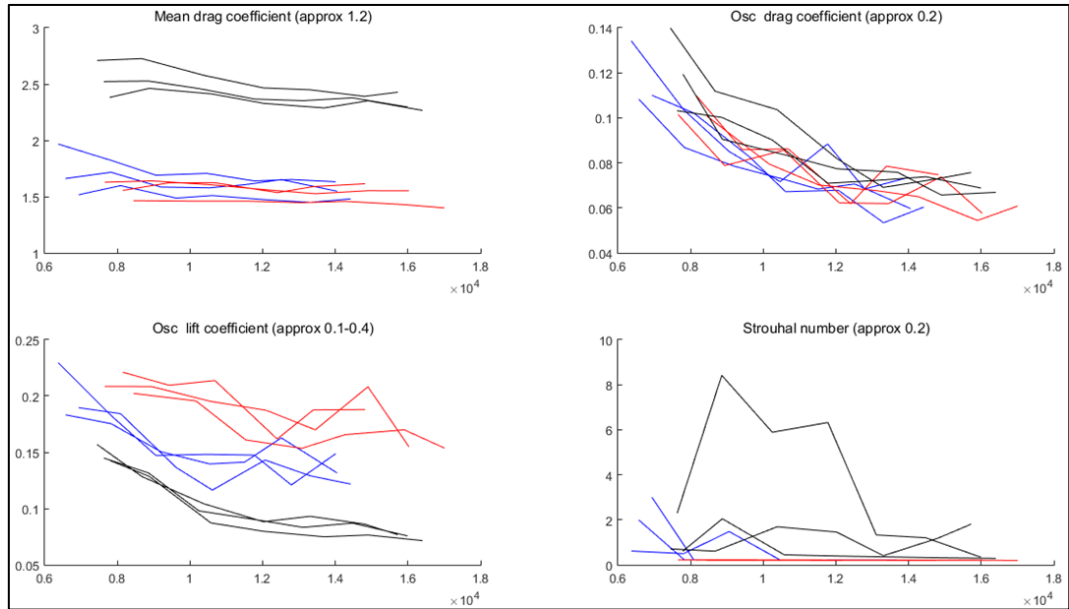
Stationary Test for Bare Pipe



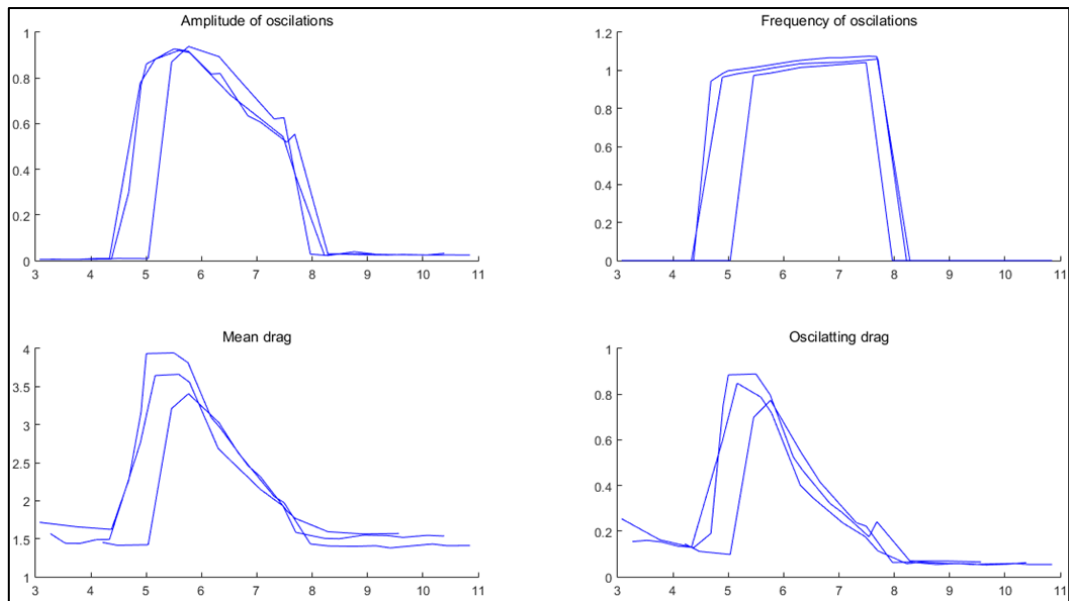
Stationary Test for Pipe with Cover



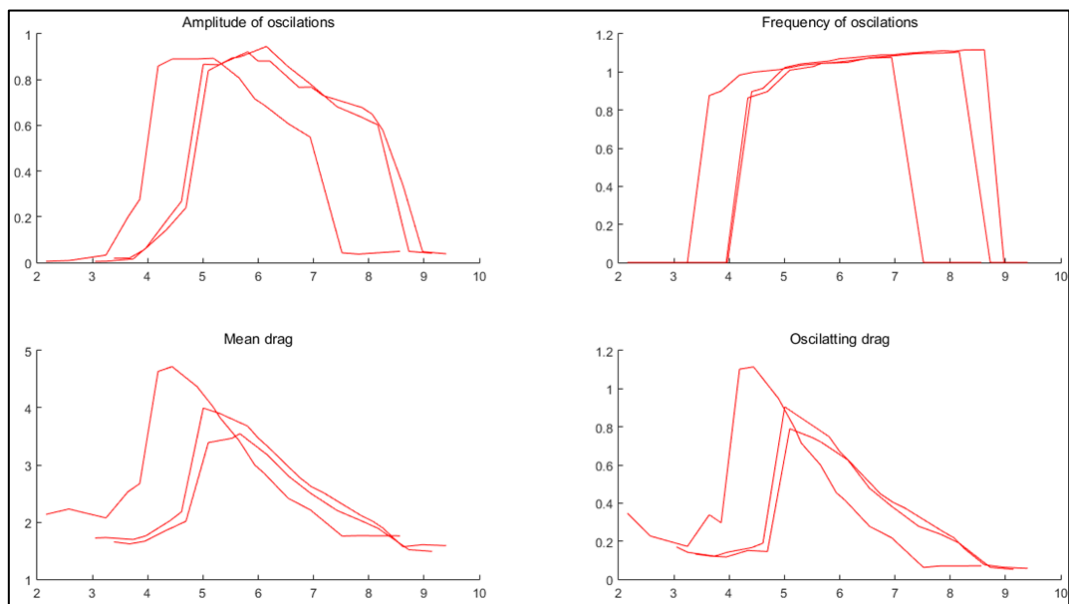
Stationary Test for Pipe with Strakes



Stationary Test for All



Free Vibration Test for Bare Pipe



Free Vibration Test for Pipe with Cover

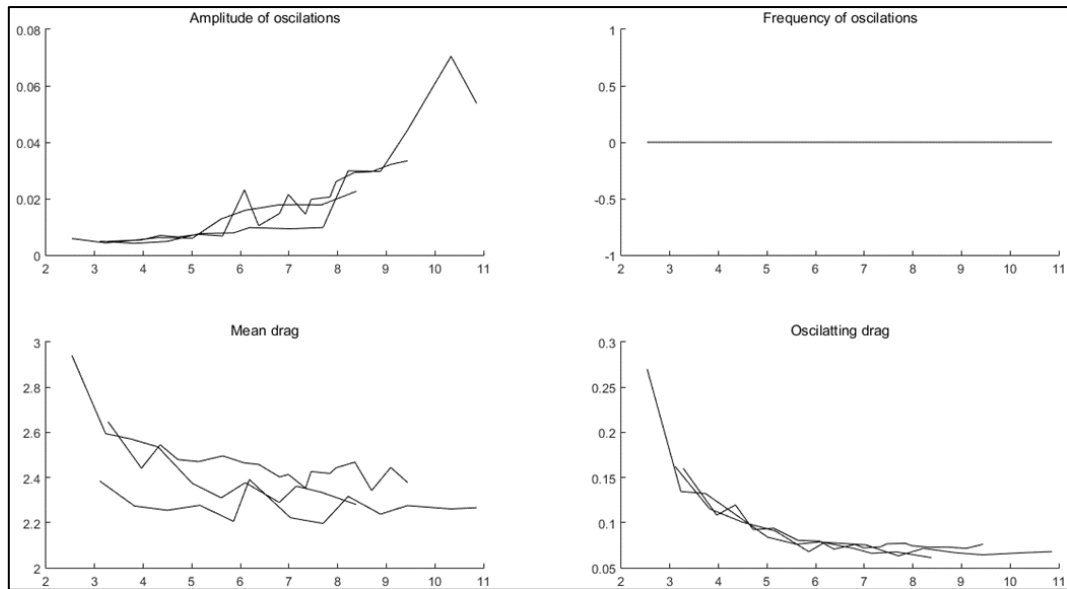


Figure 6.7 Free Vibration Test for Pipe with Strakes

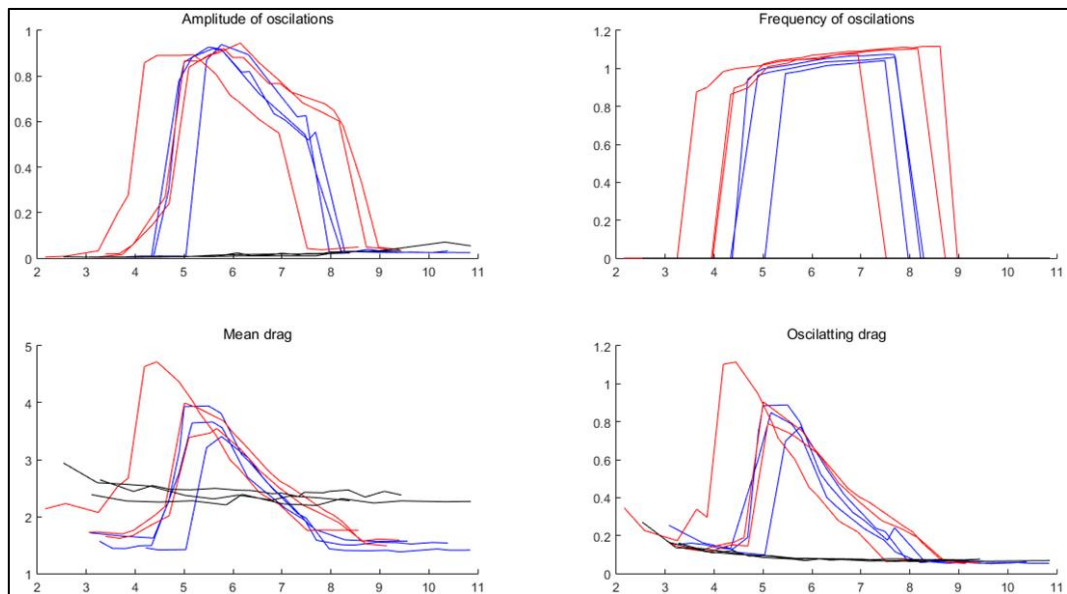


Figure 6.8 Free Vibration Test for All

Appendix B

The following figures are the simulation of the wake oscillator compared with the experiment results:

